A second order numerical scheme of the Cahn-Hilliard-Navier-Stokes system with Flory-Huggins potential

Wenbin Chen* Jianyu Jing† Qianqian Liu‡ Cheng Wang§ Xiaoming Wang¶

September 26, 2023

Abstract

A second order accurate in time, finite difference numerical scheme is proposed and analyzed for the Cahn-Hilliard-Navier-Stokes system, with logarithmic Flory-Huggins energy potential. In the numerical approximation to the chemical potential, a modified Crank-Nicolson approximation is applied to the singular logarithmic nonlinear term, while the expansive term is updated by an explicit second order Adams-Bashforth extrapolation, and an alternate temporal stencil is used for the surface diffusion term. Moreover, a nonlinear artificial regularization term is included in the chemical potential approximation, which ensures the positivity-preserving property for the logarithmic arguments, i.e., the numerical value of the phase variable is always between -1 and 1 at a point-wise level. Meanwhile, the convective term in the phase field evolutionary equation is updated in a semi-implicit way, with second order accurate temporal approximation. The fluid momentum equation is also computed by a semi-implicit algorithm. The unique solvability and the positivity-preserving property of the second order scheme is proved, accomplished by an iteration process. A modified total energy stability of the second order scheme is also derived. Some numerical results are presented to demonstrate the accuracy and the robust performance of the proposed second order scheme.

Key words and phrases: Cahn-Hilliard-Navier-Stokes system, Flory-Huggins energy potential, second order accurate numerical scheme, Crank-Nicolson approximation, positivity preserving

AMS subject classification: 35K35, 35K55, 49J40, 65M06, 65M12

1 Introduction

For simplicity, we assume the domain under consideration is the unit square $\Omega = (0,1)^2$, together with periodic boundary condition. An extension to a rectangular domain, the 3-dimensional case, or the case with homogeneous Neumann boundary condition, is straightforward.

The phase variable ϕ is assumed to have a point-wise bound, $-1 < \phi < 1$. For any $\phi \in H^1(\Omega)$ with such a bound, the Flory-Huggins free energy is formulated as

$$E(\phi) = \int_\Omega \left((1+\phi)\ln(1+\phi) + (1-\phi)\ln(1-\phi) - \frac{\theta_0}{2}\phi^2 + \frac{\epsilon^2}{2}|\nabla\phi|^2 \right) d\mathbf{x}, \tag{1.1}$$

*Shanghai Key Laboratory for Contemporary Applied Mathematics, School of Mathematical Sciences; Fudan University, Shanghai, China 200433 (wbchen@fudan.edu.cn)

†School of Mathematical Sciences; Fudan University, Shanghai, China 200433 (jyjing20@fudan.edu.cn)

‡School of Mathematical Sciences; Fudan University, Shanghai, China 200433 (qianqianliu21@m.fudan.edu.cn)

§Mathematics Department; University of Massachusetts; North Dartmouth, MA 02747 (corresponding author: cwang1@umassd.edu)

¶Department of Mathematics and Statistics, Missouri University of Science and Technology, Rolla, MO 65409, USA (xiaomingwang@mst.edu)

in which $\epsilon > 0$, $\theta_0 > 0$ are certain physical parameter constants associated with the diffuse interface width and inverse temperature, respectively; see the related references [2, 14, 17, 23].

For two phase flow problems, the fluid motion plays an important role in the physical process. A well-known two phase flow model is the following Cahn-Hilliard-Navier-Stokes (CHNS) system [36]

$$\mathbf{u}_t + \mathbf{u} \cdot \nabla \mathbf{u} + \nabla p - \nu \Delta \mathbf{u} = -\gamma \phi \nabla \mu, \tag{1.2}$$

$$\phi_t + \nabla \cdot (\phi \mathbf{u}) = \Delta \mu, \tag{1.3}$$

$$\mu := \delta_\phi E = \ln(1+\phi) - \ln(1-\phi) - \theta_0 \phi - \epsilon^2 \Delta \phi, \tag{1.4}$$

$$\nabla \cdot \mathbf{u} = 0. \tag{1.5}$$

in which $\mathbf{u}$ is the advective velocity, p is the pressure variable, and $\nu > 0$ is the kinematic viscosity. The constant $\gamma > 0$ is associated with surface tension, and term $-\gamma \phi \nabla \mu$ is a diffuse interface approximation of the singular surface force.

For such a coupled system, the following energy dissipation law can be derived:

$$E'_{total}(t) = -\int_\Omega |\nabla \mu|^2 d\mathbf{x} - \frac{\nu}{\gamma} \int_\Omega |\nabla \mathbf{u}|^2 d\mathbf{x} \le 0, \quad E_{total} = E(\phi) + \frac{1}{2\gamma} \|\mathbf{u}\|^2. \tag{1.6}$$

Many numerical works have been reported for various phase-field-fluid coupled system [3, 6, 7, 26, 27, 34, 35, 41, 42, 47, 48, 53], etc. In particular, the issue of second order accurate numerical schemes have attracted great attentions [15, 32, 54], due to its long time simulation advantages. On the other hand, most existing works of second order schemes have been based on the polynomial approximation in the energy potential. With a singular energy potential (1.1), the analysis will become much more challenging, because of the highly nonlinear, singular and coupled nature of the physical system.

In this article, we propose and analyze a second order accurate numerical scheme for the CHNS system (1.2)-(1.5), with three properties theoretically justified: positivity-preserving (for the logarithmic arguments), unique solvability, and a modified energy stability. In fact, even for the pure gradient model with singular energy potential, the works of second order accurate in time, energy stable numerical schemes are still very limited. In the numerical approximation to the chemical potential (1.4), we adopt a similar approach as in a recent work [6]: a modified Crank-Nicolson temporal discretization. More specifically, a modified Crank-Nicolson (secant-like) approximation is applied to the logarithmic nonlinear term, in the form of

$$\frac{F(1 \pm \phi^{n+1}) - F(1 \pm \phi^n)}{\phi^{n+1} - \phi^n}, \quad \text{with} \quad F(x) = x \ln x.$$

Such an approximation is convex in terms of ϕ^{n+1}, while the approximation is not singular as $\phi^{n+1} \searrow -1$ or $\phi^{n+1} \nearrow 1$. The expansive linear term is updated by a second order Adams-Bashforth explicit extrapolation formula, and an alternate temporal stencil, namely $\frac{3}{4}\Delta_h \phi^{n+1} + \frac{1}{4}\Delta_h \phi^{n-1}$, is used for the surface diffusion term. Since the singularity of the nonlinear approximation to the logarithmic term is not available as $\phi^{n+1} \searrow -1$ or $\phi^{n+1} \nearrow 1$, a nonlinear artificial regularization term has to be included in the chemical potential, namely $\Delta t(\ln(1 \pm \phi^{n+1}) - \ln(1 \pm \phi^n))$. This regularization term ensures the positivity-preserving property for both $1+\phi$ and $1-\phi$ at a theoretical level. In particular, the singular nature of the logarithmic terms around the values of -1 and 1 prevents the numerical solution reaching these limit values.

For the sake of unique solvability and energy stability properties, the other parts of the CHNS system (1.2)-(1.4) have to be computed in a semi-implicit way. In the numerical approximation to the convective term in the phase field evolution equation, explicit extrapolation formula for the

phase variable is combined with an implicit, Crank-Nicolson approximation to the velocity vector. Similar methodology is applied to the fluid momentum equation: Crank-Nicolson algorithm for the kinematic diffusion term and the fluid convection gradient term, explicit calculation for the pressure gradient, along with Adams-Bashforth extrapolation for the convection velocity. Moreover, the phase field coupled term is also updated in a semi-implicit fashion: Adams-Bashforth extrapolation for the phase variable coefficient, and the modified Crank-Nicolson approximation to the chemical potential part. As a result, an intermediate velocity field (at the next time step) is determined by this semi-implicit algorithm, which could be represented as a linear velocity solver, with a fixed chemical potential profile. Consequently, a Helmholtz projection into the divergence-free vector field is taken, which in turn yields the velocity vector and the pressure variable at the next time step. Since the Stokes solver is decoupled in this approach, the numerical efficiency is expected to be greatly improved. Some related works could also be found in [29, 37, 55], etc.

Because of the coupled and non-symmetric feature of the numerical system, the unique solvability and positivity-preserving analysis for the proposed second order scheme is expected to be much more challenging than the one for the pure phase field gradient flow. In more details, the proposed numerical system could not be represented as a minimization of a discrete energy functional, which comes from the non-symmetric nature of the fluid convection term in the Navier-Stokes equation. As a result, many well-established techniques to deal with singular energy potential gradient flows [6, 10] are not directly applicable. On the other hand, the Browder-Minty lemma [1, 43] has been a well-known tool to deal with nonlinear, monotone, while non-symmetric systems. However, a direct application of this analysis is not feasible, since the singularity of the logarithmic terms destroys the coercivity condition for the phase variable. To overcome these subtle difficulties, we have to construct an iteration process to accomplish the theoretical analysis. First, it is observed that the intermediate velocity vector could be represented as a non-symmetric, linear operator in terms of a fixed chemical potential profile. The convection-diffusion nature of this linear operator implies its monotonicity property. Therefore, a substitution into the numerical algorithm for the phase variable evolutionary equation leads to an alternate representation of the chemical potential variable: a non-symmetric, linear operator of the discrete temporal derivative of the phase variable. A combination with the modified Crank-Nicolson approximation for the chemical potential results in a closed system for the phase variable. This nonlinear system is monotone in terms of the phase variable, while the logarithmic terms prevent a direct application of the Browder-Minty analysis. Instead, a nonlinear iteration is constructed: at each iteration stage, the non-symmetric, linear operator of the discrete temporal derivative part is explicitly treated as a source term, while all other terms are implicitly solved. In addition, a relaxation algorithm is included at each iteration stage. Since all the implicit terms in the iteration stage, including the singular logarithmic terms, have symmetric Jacobian matrix, a discrete energy minimization approach is available, so that the proposed iteration process creates a unique solution satisfying the positivity-preserving property at each iteration stage; also see the related works [6, 10]. Combined with the monotonicity analysis for the linear operator of the discrete temporal derivative, a contraction mapping estimate of this nonlinear iteration could be carefully derived. Consequently, a fixed point argument would be available, and the unique solvability/positivity-preserving property (for the logarithmic arguments) could be proved.

With a unique solution to the proposed numerical system available, preserving a point-wise positivity, the total energy stability analysis of the second order scheme turns out to be more straightforward. By taking discrete inner product with the evolutionary equation for the phase field variable and the momentum equation by the associated test variables, we are able to obtain a dissipation law for the discrete functional of the total energy, combined with a few numerical correction terms. These correction terms come from the second order temporal approximation, as

well as the decoupled Stokes solver. In the analysis for the fully discrete scheme, the summation by parts formulas for different physical variables, combined with the staggered location of these variables, will play an important role.

The rest of the article is organized as follows. In Section 2 we review the finite difference spatial approximation, and propose the second order numerical scheme. The unique solvability and the positivity-preserving analysis is provided in Section 3. A modified total energy stability estimate is established in Section 4. Some numerical results are presented in Section 5, and the concluding remarks are given in Section 6.

2 Numerical scheme

2.1 The finite difference spatial discretization

For simplicity, we only consider the two dimensional domain $\Omega = (0,1)^2$. The three dimensional case can be similarly extended.

Let N be a positive integer and define the uniform spatial grid size $h = \frac{1}{N}$. We now introduce the standard marker and cell (MAC) grid [33], where the phase variable ϕ, the chemical potential μ and the pressure field p are defined on the cell-centered mesh points $\left(\left(i+\frac{1}{2}\right)h,\ \left(j+\frac{1}{2}h\right)\right),\ 0 \le i,\ j \le N$. Meanwhile, given a velocity field $\mathbf{u} = (u^x,\ u^y)$, the x-component of the velocity will be defined at the east-west cell edge points $\left(ih,\ \left(j+\frac{1}{2}h\right)\right),\ 0 \le i \le N+1,\ 0 \le j \in \le N$, while the y-component of the velocity is located at the north-south cell edge points $\left(\left(i+\frac{1}{2}\right)h,\ jh\right)$.

For a function $f(x,y)$, denote $f_{i+\frac{1}{2},j+\frac{1}{2}}$ as the value of $f\left(\left(i+\frac{1}{2}\right)h,\ \left(j+\frac{1}{2}\right)h\right)$. The notations $f_{i+\frac{1}{2},j}$, $f_{i,j+\frac{1}{2}}$ could be similarly introduced. Then the following difference operators are defined:

$$(D_x^c f)_{i,j+\frac{1}{2}} = \frac{f_{i+\frac{1}{2},j+\frac{1}{2}} - f_{i-\frac{1}{2},j+\frac{1}{2}}}{h}, \qquad (D_y^c f)_{i+\frac{1}{2},j} = \frac{f_{i+\frac{1}{2},j+\frac{1}{2}} - f_{i+\frac{1}{2},j-\frac{1}{2}}}{h}, \tag{2.1}$$

$$(D_x^{ew} f)_{i+\frac{1}{2},j+\frac{1}{2}} = \frac{f_{i+1,j+\frac{1}{2}} - f_{i,j+\frac{1}{2}}}{h}, \qquad (D_y^{ew} f)_{i,j} = \frac{f_{i,j+\frac{1}{2}} - f_{i,j-\frac{1}{2}}}{h}, \tag{2.2}$$

$$(D_x^{ns} f)_{i,j} = \frac{f_{i+\frac{1}{2},j} - f_{i-\frac{1}{2},j}}{h}, \qquad (D_y^{ns} f)_{i+\frac{1}{2},j+\frac{1}{2}} = \frac{f_{i+\frac{1}{2},j+1} - f_{i+\frac{1}{2},j}}{h}. \tag{2.3}$$

Such definitions may vary on the boundary, if implemented with different boundary conditions. Specifically, with periodic boundary condition, (2.1) becomes

$$(D_x^c f)_{0,j+\frac{1}{2}} = (D_x^c f)_{N,j+\frac{1}{2}} = \frac{f_{\frac{1}{2},j+\frac{1}{2}} - f_{N-\frac{1}{2},j+\frac{1}{2}}}{h}, \tag{2.4}$$

$$(D_y^c f)_{i+\frac{1}{2},0} = (D_y^c f)_{i+\frac{1}{2},N} = \frac{f_{i+\frac{1}{2},\frac{1}{2}} - f_{i-\frac{1}{2},N-\frac{1}{2}}}{h}. \tag{2.5}$$

For (2.2)-(2.3), the formula can be analogously derived. As for homogeneous Neumann boundary condition, (2.1) becomes

$$(D_x^c f)_{0,j+\frac{1}{2}} = (D_x^c f)_{N,j+\frac{1}{2}} = (D_y^c f)_{i+\frac{1}{2},0} = (D_y^c f)_{i+\frac{1}{2},N} = 0. \tag{2.6}$$

Finally, with the homogeneous Neumann boundary condition, a ghost point is needed and and will be eliminated using linear interpolation of the boundary conditions, so that (2.2)-(2.3) become

$$(D_y^{ew} f)_{i,0} = \frac{f_{i,\frac{1}{2}} - f_{i,-\frac{1}{2}}}{h} = \frac{2f_{i,\frac{1}{2}}}{h}, \qquad (D_y^{ew} f)_{i,N} = \frac{f_{i,N+\frac{1}{2}} - f_{i,N-\frac{1}{2}}}{h} = -\frac{2f_{i,N-\frac{1}{2}}}{h}, \tag{2.7}$$

$$(D_x^{ns} f)_{0,j} = \frac{f_{\frac{1}{2},j} - f_{-\frac{1}{2},j}}{h} = \frac{2f_{\frac{1}{2},j}}{h}, \qquad (D_x^{ns} f)_{N,j} = \frac{f_{N+\frac{1}{2},j} - f_{N-\frac{1}{2},j}}{h} = -\frac{2f_{N-\frac{1}{2},j}}{h}. \tag{2.8}$$

We also introduce the long stencil difference operator, defined on the east-west cell edge points and north-south cell edge points:

$$(\tilde{D}_x f)_{i,\,j+\frac{1}{2}} = \frac{f_{i+1,\,j+\frac{1}{2}} - f_{i-1,\,j+\frac{1}{2}}}{2h}, \qquad (\tilde{D}_y f)_{i+\frac{1}{2},\,j} = \frac{f_{i+\frac{1}{2},\,j+1} - f_{i+\frac{1}{2},\,j-1}}{2h}. \tag{2.9}$$

Again, the definitions are slightly different on the boundary. When equipped with periodic boundary condition, (2.9) becomes

$$(\tilde{D}_x f)_{0,\,j+\frac{1}{2}} = (\tilde{D}_x f)_{N,\,j+\frac{1}{2}} = \frac{f_{1,\,j+\frac{1}{2}} - f_{N-1,\,j+\frac{1}{2}}}{2h}, \tag{2.10}$$

$$(\tilde{D}_y f)_{i+\frac{1}{2},\,0} = (\tilde{D}_y f)_{i+\frac{1}{2},\,N} = \frac{f_{i+\frac{1}{2},\,1} - f_{i+\frac{1}{2},\,N-1}}{2h}. \tag{2.11}$$

With homogeneous Neumann boundary condition, (2.9) becomes

$$(\tilde{D}_x f)_{0,\,j+\frac{1}{2}} = \frac{f_{1,\,j+\frac{1}{2}} - f_{-1,\,j+\frac{1}{2}}}{2h} = \frac{f_{1,\,j+\frac{1}{2}}}{h}, \tag{2.12}$$

$$(\tilde{D}_x f)_{N,\,j+\frac{1}{2}} = \frac{f_{N+1,\,j+\frac{1}{2}} - f_{N-1,\,j+\frac{1}{2}}}{2h} = -\frac{f_{N-1,\,j+\frac{1}{2}}}{h}, \tag{2.13}$$

$$(\tilde{D}_y f)_{i+\frac{1}{2},\,0} = \frac{f_{i+\frac{1}{2},\,1} - f_{i+\frac{1}{2},\,-1}}{2h} = \frac{f_{i+\frac{1}{2},\,1}}{h}, \tag{2.14}$$

$$(\tilde{D}_y f)_{i+\frac{1}{2},\,N} = \frac{f_{i+\frac{1}{2},\,N+1} - f_{i+\frac{1}{2},\,N-1}}{2h} = -\frac{f_{i+\frac{1}{2},\,N-1}}{h}. \tag{2.15}$$

For a grid function f, the discrete gradient operator is defined as follows:

$$\nabla_h f_h = \Big((D_x^{\ell} f),\ (D_y^{\ell} f) \Big)^T, \tag{2.16}$$

where $\ell = c,\ ew,\ ns$ may depend on the choice of f. The discrete divergence operator of a vector gird function $\mathbf{u}$, defined on the cell-centered points, is given by

$$(\nabla_h \cdot \mathbf{u})_{i+\frac{1}{2},\,j+\frac{1}{2}} = (D_x^{ew} u^x)_{i+\frac{1}{2},\,j+\frac{1}{2}} + (D_y^{ns} u^y)_{i+\frac{1}{2},\,j+\frac{1}{2}}. \tag{2.17}$$

In turn, the five-point standard Laplacian operator is defined as

$$(\Delta_h f)_{r,\,s} = \frac{f_{r+1,\,s} + f_{r-1,\,s} + f_{r,\,s+1} + f_{r,\,s-1} - 4 f_{r,\,s}}{h^2}, \tag{2.18}$$

where $(r,\, s)$ may refer to $(i + \frac{1}{2},\, j + \frac{1}{2})$, $(i + \frac{1}{2},\, j)$ and $(i,\, j + \frac{1}{2})$.

For $\mathbf{u} = (u^x,\, u^y)^T$, $\mathbf{v} = (v^x,\, v^y)^T$, located at the staggered mesh points respectively, and the cell centered variables ϕ, μ, the nonlinear terms are evaluated as follows:

$$\mathbf{u} \cdot \nabla_h \mathbf{v} = \begin{pmatrix} u^x_{i,\,j+\frac{1}{2}} \tilde{D}_x v^x_{i,\,j+\frac{1}{2}} + \mathcal{A}_{xy} u^y_{i,\,j+\frac{1}{2}} \tilde{D}_y v^x_{i,\,j+\frac{1}{2}} \\ \mathcal{A}_{xy} u^x_{i+\frac{1}{2},\,j} \tilde{D}_x v^y_{i+\frac{1}{2},\,j} + u^y_{i,\,j+\frac{1}{2}} \tilde{D}_y v^y_{i+\frac{1}{2},\,j} \end{pmatrix}, \tag{2.19}$$

$$\nabla_h \cdot (\mathbf{v}\mathbf{u}^T) = \begin{pmatrix} \tilde{D}_x (u^x v^x)_{i,\,j+\frac{1}{2}} + \tilde{D}_y (\mathcal{A}_{xy} u^y v^x)_{i,\,j+\frac{1}{2}} \\ \tilde{D}_x (\mathcal{A}_{xy} u^x v^y)_{i+\frac{1}{2},\,j} + \tilde{D}_y (u^y v^y)_{i+\frac{1}{2},\,j} \end{pmatrix}, \tag{2.20}$$

$$\mathcal{A}_h \phi \nabla_h \mu = \begin{pmatrix} (D_x^c \mu \cdot \mathcal{A}_x \phi)_{i,\,j+\frac{1}{2}} \\ (D_y^c \mu \cdot \mathcal{A}_y \phi)_{i+\frac{1}{2},\,j} \end{pmatrix}, \tag{2.21}$$

$$\nabla_h \cdot (\mathcal{A}_h \phi \mathbf{u}) = D_x^{ew} (u^x \mathcal{A}_x \phi)_{i+\frac{1}{2},\,j+\frac{1}{2}} + D_y^{ns} (u^y \mathcal{A}_y \phi)_{i+\frac{1}{2},\,j+\frac{1}{2}}, \tag{2.22}$$

where the following averaging operators have been introduced:

$$\mathcal{A}_{xy}u^x_{i+\frac{1}{2},j} = \frac{1}{4}\left(u^x_{i,j-\frac{1}{2}} + u^x_{i,j+\frac{1}{2}} + u^x_{i+1,j-\frac{1}{2}} + u^x_{i+1,j+\frac{1}{2}}\right), \tag{2.23}$$

$$\mathcal{A}_x\phi_{i,j+\frac{1}{2}} = \frac{1}{2}\left(\phi_{i-\frac{1}{2},j+\frac{1}{2}} + \phi_{i+\frac{1}{2},j+\frac{1}{2}}\right). \tag{2.24}$$

A few other average terms, such as $\mathcal{A}_{xy}u^y_{i,j+\frac{1}{2}}$, $\mathcal{A}_y\phi_{i+\frac{1}{2},j}$, could be similarly defined.

We now prepare to give the definition of discrete inner product. Let f, g be two grid functions defined on the cell-center points, the discrete ℓ^2 inner product is given by

$$\langle f, g\rangle_c = h^2\sum_{i=1}^{N}\sum_{j=1}^{N} f_{i+\frac{1}{2},j+\frac{1}{2}}g_{i+\frac{1}{2},j+\frac{1}{2}}. \tag{2.25}$$

If f, g are evaluated on the east-west points, (2.25) becomes:

$$\langle f, g\rangle_{ew} = h^2\sum_{i=1}^{N}\sum_{j=1}^{N} f_{i,j+\frac{1}{2}}g_{i,j+\frac{1}{2}}. \tag{2.26}$$

If f, g are evaluated on the north-south points, (2.25) shifts into:

$$\langle f, g\rangle_{ns} = h^2\sum_{i=1}^{N}\sum_{j=1}^{N} f_{i+\frac{1}{2},j}g_{i+\frac{1}{2},j}. \tag{2.27}$$

Moreover, for two vector grid functions $\mathbf{u} = (u^x,\, u^y)^T$, $\mathbf{v} = (v^x,\, v^y)^T$ whose components are defined on east-west and north-south respectively, the vector inner product is introduced:

$$\langle \mathbf{u}, \mathbf{v}\rangle_1 = \langle u^x, v^x\rangle_{ew} + \langle u^y, v^y\rangle_{ns}. \tag{2.28}$$

In turn, the discrete ℓ^2 norms, $\|\cdot\|_2$ can be naturally induced. Moreover, the discrete ℓ^p $(1 \le p \le \infty)$ norms are needed in the later analysis. For $(r,\, s) = (i+\frac{1}{2},\, j+\frac{1}{2})$, $(i+\frac{1}{2},\, j)$ or $(i,\, j+\frac{1}{2})$, we denote

$$\|f\|_\infty := \max_{r,\,s}|f_{r,s}|, \qquad \|f\|_p := \left(h^2\sum_{r=0}^{N}\sum_{s=0}^{N}|f_{r,s}|^p\right)^{\frac{1}{p}}, \quad 1 \le p < \infty. \tag{2.29}$$

Finally, the following summation by parts formula is recalled and will be useful in the later analysis.

Lemma 2.1. *For two discrete grid vector functions $\boldsymbol{u} = (u^x,\, u^y)$, $\boldsymbol{v} = (v^x,\, v^y)$, where u^x, u^y and v^x, v^y are defined on east-west and north-south respectively, and two cell centered functions f, g, the following identities are valid, if $\boldsymbol{u}$, $\boldsymbol{v}$, f, g are equipped with periodic boundary condition, or $\boldsymbol{u}$, $\boldsymbol{v}$ are implemented with homogeneous Dirichlet boundary condition and homogeneous Neumann boundary condition is imposed for f and g:*

$$\langle \boldsymbol{v}, \boldsymbol{u}\cdot\nabla_h\boldsymbol{v}\rangle_1 + \left\langle \boldsymbol{v}, \nabla_h\cdot(\boldsymbol{v}\boldsymbol{u}^T)\right\rangle_1 = 0, \tag{2.30}$$

$$\langle \boldsymbol{u}, \nabla_h f\rangle_1 = 0, \quad \text{if } \nabla_h\cdot\boldsymbol{u} = 0, \tag{2.31}$$

$$-\langle \boldsymbol{v}, \Delta_h\boldsymbol{v}\rangle_1 = \|\nabla_h\boldsymbol{v}\|_2^2, \tag{2.32}$$

$$-\langle f, \Delta_h f\rangle_c = \|\nabla_h f\|_2^2, \tag{2.33}$$

$$-\langle g, \nabla_h\cdot(\mathcal{A}_h f\,\boldsymbol{u})\rangle_c = \langle \boldsymbol{u}, \mathcal{A}_h f\nabla_h g\rangle_1. \tag{2.34}$$

2.2 The proposed second order accurate numerical scheme

Here we propose the second order in time Crank-Nicolson scheme as follows. Given $\mathbf{u}^n = ((u^x)^n, (u^y)^n)$, $\mathbf{u}^{n-1} = \left((u^x)^{n-1}, (u^y)^{n-1}\right)$ evaluated at the MAC staggered grid, and p^n, ϕ^n, ϕ^{n-1} located at the cell-centered grid, with $\|\phi^n\|_\infty$, $\left\|\phi^{n-1}\right\|_\infty < 1$, we aim to find $\hat{\mathbf{u}}^{n+1}$, $\mathbf{u}^{n+1}$, p^{n+1}, ϕ^{n+1} that satisfy

$$\begin{aligned}
&\frac{\hat{\mathbf{u}}^{n+1}-\mathbf{u}^n}{\tau} + \frac{1}{2}\left(\tilde{\mathbf{u}}^{n+\frac{1}{2}}\cdot\nabla_h\bar{\hat{\mathbf{u}}}^{n+\frac{1}{2}} + \nabla_h\cdot\left(\bar{\hat{\mathbf{u}}}^{n+\frac{1}{2}}(\tilde{\mathbf{u}}^{n+\frac{1}{2}})^T\right)\right) + \nabla_h p^n - \nu\Delta_h\bar{\hat{\mathbf{u}}}^{n+\frac{1}{2}} \\
&\quad = -\gamma\mathcal{A}_h\tilde{\phi}^{n+\frac{1}{2}}\nabla_h\mu^{n+\frac{1}{2}}, \qquad (2.35)\\
&\frac{\phi^{n+1}-\phi^n}{\tau} + \nabla_h\cdot\left(\mathcal{A}_h\tilde{\phi}^{n+\frac{1}{2}}\bar{\hat{\mathbf{u}}}^{n+\frac{1}{2}}\right) = \Delta_h\mu^{n+\frac{1}{2}}, \qquad (2.36)\\
&\mu^{n+\frac{1}{2}} = \frac{G(1+\phi^{n+1})-G(1+\phi^n)}{\phi^{n+1}-\phi^n} + \frac{G(1-\phi^{n+1})-G(1-\phi^n)}{\phi^{n+1}-\phi^n} - \theta_0\tilde{\phi}^{n+\frac{1}{2}} - \epsilon^2\Delta_h\bar{\bar{\phi}}^{n+\frac{1}{2}} \\
&\qquad + \tau\left(\ln(1+\phi^{n+1}) - \ln(1+\phi^n) - \ln(1-\phi^{n+1}) + \ln(1-\phi^n)\right), \qquad (2.37)\\
&\frac{\mathbf{u}^{n+1}-\hat{\mathbf{u}}^{n+1}}{\tau} + \frac{1}{2}\nabla_h(p^{n+1}-p^n) = 0, \qquad (2.38)\\
&\nabla_h\cdot\mathbf{u}^{n+1} = 0, \qquad (2.39)
\end{aligned}$$

where

$$\begin{aligned}
&\tilde{\phi}^{n+\frac{1}{2}} := \frac{3}{2}\phi^n - \frac{1}{2}\phi^{n-1}, \quad \bar{\phi}^{n+\frac{1}{2}} := \frac{1}{2}\phi^{n+1} + \frac{1}{2}\phi^n, \quad \bar{\bar{\phi}}^{n+\frac{1}{2}} := \frac{3}{4}\phi^{n+1} + \frac{1}{4}\phi^{n-1},\\
&\tilde{\mathbf{u}}^{n+\frac{1}{2}} := \frac{3}{2}\mathbf{u}^n - \frac{1}{2}\mathbf{u}^{n-1}, \quad \bar{\hat{\mathbf{u}}}^{n+\frac{1}{2}} := \frac{1}{2}\hat{\mathbf{u}}^{n+1} + \frac{1}{2}\mathbf{u}^n, \quad G(x) = x\ln(x),
\end{aligned} \qquad (2.40)$$

for either periodic boundary condition, or the physical boundary condition:

$$\hat{\mathbf{u}}^{n+1}|_\Gamma = 0, \quad \mathbf{u}^{n+1}\cdot\mathbf{n} = 0, \quad \partial_n\phi^{n+1}|_\Gamma = \partial_n\mu^{n+\frac{1}{2}}|_\Gamma = 0. \qquad (2.41)$$

Remark 2.1. *The numerical method* (2.36)-(2.39) *doesn't give a way on how to calculate the first step value. In fact, the first step variable* ϕ^1, $\boldsymbol{u}^1$, p^1 *can be either calculated using a ghost point* $\phi^{-1} = \phi^0$, $\boldsymbol{u}^{-1} = \boldsymbol{u}^0$ *(which is first order accurate in the initial step), or using other higher order algorithm, such as Runge-Kutta method.*

Clearly, the phase variable satisfies the mass conservation property, i.e.,

$$\overline{\phi^{n+1}} = \overline{\phi^n} = \cdots = \overline{\phi^0}. \qquad (2.42)$$

For simplicity, the following smooth function is introduced: for any $a > 0$,

$$F_a(x) := \frac{G(x)-G(a)}{x-a}, \ \forall x > 0. \qquad (2.43)$$

In turn, (2.37) can be rewritten as:

$$\begin{aligned}
\mu^{n+\frac{1}{2}} &= F_{1+\phi^n}(1+\phi^{n+1}) - F_{1-\phi^n}(1-\phi^{n+1}) - \theta_0\tilde{\phi}^{n+\frac{1}{2}} - \epsilon^2\Delta_h\bar{\bar{\phi}}^{n+\frac{1}{2}} \\
&\quad + \tau\left(\ln(1+\phi^{n+1}) - \ln(1+\phi^n) - \ln(1-\phi^{n+1}) + \ln(1-\phi^n)\right).
\end{aligned} \qquad (2.44)$$

The following lemma is useful in the later analysis:

Lemma 2.2. *[6] Let* $a > 0$ *be fixed, then*

1. $F_a'(x) = \frac{G'(x)(x-a)-(G(x)-G(a))}{(x-a)^2} \geq 0$, *for any* $x > 0$.
2. $F_a(x)$ *is an increasing function of* x, *and* $F_a(x) \leq F_a(a) = \ln a + 1$ *for any* $0 < x < a$.

3 The unique solvability and positivity-preserving property

The unique solvability and positivity preserving analysis is based on four steps.

Step 1: We first establish the connection between $\hat{\mathbf{u}}^{n+1}$ and $\mu^{n+\frac{1}{2}}$. Observe that (2.35) is equivalent to

$$\begin{aligned}
&\frac{2\bar{\hat{\mathbf{u}}}^{n+\frac{1}{2}} - 2\mathbf{u}^n}{\tau} + \frac{1}{2}\left(\tilde{\mathbf{u}}^{n+\frac{1}{2}} \cdot \nabla_h \bar{\hat{\mathbf{u}}}^{n+\frac{1}{2}} + \nabla_h \cdot \left(\bar{\hat{\mathbf{u}}}^{n+\frac{1}{2}} (\tilde{\mathbf{u}}^{n+\frac{1}{2}})^T\right)\right) + \nabla_h p^n - \nu \Delta_h \bar{\hat{\mathbf{u}}}^{n+\frac{1}{2}} \\
&\quad = -\gamma \mathcal{A}_h \tilde{\phi}^{n+\frac{1}{2}} \nabla_h \mu^{n+\frac{1}{2}}, \qquad (3.1)\\
&\hat{\mathbf{u}}^{n+1} = 2\bar{\hat{\mathbf{u}}}^{n+\frac{1}{2}} - \mathbf{u}^n. \qquad (3.2)
\end{aligned}$$

In other words, for a given field μ, we could define $\mathbf{v} = \mathcal{L}_h^{NS}(\mu)$ as the unique solution of the following discrete convection-diffusion equation:

$$\frac{2\mathbf{v} - 2\mathbf{u}^n}{\tau} + \frac{1}{2}\left(\tilde{\mathbf{u}}^{n+\frac{1}{2}} \cdot \nabla_h \mathbf{v} + \nabla_h \cdot \left(\mathbf{v}(\tilde{\mathbf{u}}^{n+\frac{1}{2}})^T\right)\right) + \nabla_h p^n - \nu \Delta_h \mathbf{v} = -\gamma \mathcal{A}_h \tilde{\phi}^{n+\frac{1}{2}} \nabla_h \mu. \qquad (3.3)$$

Then we obtain $\bar{\hat{\mathbf{u}}}^{n+\frac{1}{2}} = \mathcal{L}_h^{NS}(\mu^{n+\frac{1}{2}})$, and $\hat{\mathbf{u}}^{n+1}$ could be updated by the formula (3.2). In turn, $\mathbf{u}^{n+1}$ becomes the discrete Helmholtz projection of $\hat{\mathbf{u}}^{n+1}$ into divergence-free space.

Step 2: We next establish the connection between ϕ^{n+1} and $\mu^{n+\frac{1}{2}}$. A substitution of $\bar{\hat{\mathbf{u}}}^{n+\frac{1}{2}} = \mathcal{L}_h^{NS}(\mu^{n+\frac{1}{2}})$ into (2.36) leads to

$$\frac{\phi^{n+1} - \phi^n}{\tau} + \nabla_h \cdot \left(\mathcal{A}_h \tilde{\phi}^{n+\frac{1}{2}} \mathcal{L}_h^{NS}(\mu^{n+\frac{1}{2}})\right) = \Delta_h \mu^{n+\frac{1}{2}}. \qquad (3.4)$$

Define $\mathcal{L}_h^{CH}$: $(\mathbb{R}^{N^2})^2 \to (\mathbb{R}^{N^2})^2$ to be:

$$\mathcal{L}_h^{CH}(\mu) = \nabla_h \cdot \left(\mathcal{A}_h \tilde{\phi}^{n+\frac{1}{2}} \mathcal{L}_h^{NS}(\mu)\right) - \Delta_h \mu. \qquad (3.5)$$

Observe that $\mathcal{L}_h^{CH}$ is a linear operator, with either periodic, or homogeneous Neumann boundary condition imposed. Subsequently, (3.4) can be represented as

$$\frac{\phi^{n+1} - \phi^n}{\tau} = -\mathcal{L}_h^{CH}(\mu^{n+\frac{1}{2}}). \qquad (3.6)$$

Step 3: To proceed the analysis, we rewrite (3.6) as

$$\frac{1}{\tau}(\mathcal{L}_h^{CH})^{-1}(\phi^{n+1} - \phi^n) + \mu^{n+\frac{1}{2}} = 0. \qquad (3.7)$$

To make (3.7) well defined, we must show that the operator $\mathcal{L}_h^{CH}$ is invertible. Following the proof of Lemma 3.2 and Proposition 3.1 in [5], we can derive the next two properties of $\mathcal{L}_h^{CH}$.

Proposition 3.1. *[5] The linear operator $\mathcal{L}_h^{CH}$ satisfies the monotonicity condition:*

$$\left\langle \mathcal{L}_h^{CH}(\mu_1) - \mathcal{L}_h^{CH}(\mu_2), \mu_1 - \mu_2 \right\rangle_c \geq \|\nabla_h(\mu_1 - \mu_2)\|^2 \geq 0, \qquad (3.8)$$

for any μ_1, μ_2. In addition, equality is realized if and only if $\mu_1 = \mu_2$, if we require $\overline{\mu_1} = \overline{\mu_2} = 0$. Therefore, the operator $\mathcal{L}_h^{CH}$ is invertible.

Proposition 3.2. *[5] The linear operator $(\mathcal{L}_h^{CH})^{-1}$ also satisfies the monotonicity condition:*

$$\left\langle (\mathcal{L}_h^{CH})^{-1}(\phi_1), (\mathcal{L}_h^{CH})^{-1}(\phi_2) \right\rangle_c \geq \left\| \nabla_h \left((\mathcal{L}_h^{CH})^{-1}(\phi_1 - \phi_2) \right) \right\|^2 \geq C_1^2 \left\| (\mathcal{L}_h^{CH})^{-1}(\phi_1 - \phi_2) \right\|^2 \quad (3.9)$$

for any ϕ_1, ϕ_2, with $\overline{\phi_1} = \overline{\phi_2} = 0$. The constant C_1 with the discrete elliptic regularity

$$\|\nabla_h f\| \geq C_1 \|f\|, \text{ for any } f \text{ with } \overline{f} = 0, \quad (3.10)$$

with C_1 only dependent on Ω. In addition, the equality is valid if and only if $\phi_1 = \phi_2$.

A combination of (2.37) and (3.7) leads to

$$\begin{aligned} \frac{1}{\tau}(\mathcal{L}_h^{CH})^{-1}(\phi^{n+1} - \phi^n) + F_{1+\phi^n}(1 + \phi^{n+1}) + F_{1+\phi^n}(1 - \phi^{n+1}) - \theta_0 \tilde{\phi}^{n+\frac{1}{2}} - \epsilon^2 \Delta_h \bar{\bar{\phi}}^{n+\frac{1}{2}} \\ + \tau \left(\ln(1 + \phi^{n+1}) - \ln(1 + \phi^n) - \ln(1 - \phi^{n+1}) + \ln(1 - \phi^n) \right) = 0. \end{aligned} \quad (3.11)$$

For the unique solvability analysis, we also need a discrete ℓ^2 and ℓ^∞ estimate for the operator $(\mathcal{L}_h^{CH})^{-1}$. Notice that the $(\mathcal{L}_h^{CH})$ can be decomposed into

$$\mathcal{L}_h^{CH}(\mu) = \mathcal{L}_{h,1}(\mu) + \mathcal{L}_{h,2}, \text{ where } \mathcal{L}_{h,2} := \nabla_h \cdot \left(\mathcal{A}_h \tilde{\phi}^{n+\frac{1}{2}} \left(\mathbf{u}^n - \frac{\tau}{2} \nabla_h p^n \right) \right), \text{ for any } \overline{\mu} = 0, \quad (3.12)$$

in which $\mathcal{L}_{h,1}$ corresponds to the homogeneous linear operator. Since the non-homogeneous source term only depends on the numerical solution in the previous two time steps, we see that

$$\|\mathcal{L}_{h,2}\| \leq C_0, \text{ where } C_0 \text{ depends on } \tau, \ \phi^n, \ \phi^{n-1}, \ \mathbf{u}^n \text{ and } p^n. \quad (3.13)$$

The following estimate could also be derived in a similar manner as in [5].

Proposition 3.3. *[5] for any ϕ with $\overline{\phi} = 0$, the following $\|\cdot\|$ and $\|\cdot\|_\infty$ bounds are valid:*

$$\left\| (\mathcal{L}_h^{CH})^{-1}(\phi) \right\| \leq C_1^{-2} \left(\|\phi\| + C_0 \right), \quad (3.14)$$

$$\left\| (\mathcal{L}_h^{CH})^{-1}(\phi) \right\|_\infty \leq C_1^{-2} h^{-\frac{d}{2}} \left(\|\phi\| + C_0 \right). \quad (3.15)$$

Step 4: We will establish the existence of ϕ^{n+1} in (3.11), which is also the key point to this proof. Since $(\mathcal{L}_h^{CH})^{-1}$ is not a symmetric operator, we can not directly apply the discrete energy minimization technique. On the other hand, due to the singularity of $\ln(1 \pm \phi)$ when $\phi \to \mp 1$, the Browder-Minty lemma is not directly applicable to this system, either. In turn, we seek to construct a fixed point sequence to get the result.

Define the nonlinear iteration:

$$\begin{aligned} \mathcal{G}_h(\phi^{(m+1)}) :=& F_{1+\phi^n}(1 + \phi^{(m+1)}) - F_{1-\phi^n}(1 - \phi^{(m+1)}) - \epsilon^2 \Delta_h \left(\frac{3}{4}\phi^{(m+1)} + \frac{1}{4}\phi^{n-1} \right) \\ &+ \tau \left(\ln(1 + \phi^{(m+1)}) - \ln(1 + \phi^n) - \ln(1 - \phi^{(m+1)}) + \ln(1 - \phi^n) \right) \\ &- \theta_0 \tilde{\phi}^{n+\frac{1}{2}} + A\phi^{(m+1)} \\ =& -\frac{1}{\tau}(\mathcal{L}_h^{CH})^{-1}(\phi^{(m)} - \phi^n) + A\phi^{(m)}, \text{ with } \phi^{(0)} = \phi^n, \end{aligned} \quad (3.16)$$

where $A > 0$ is a constant. The following proposition ensures the existence of the solution $\phi^{(m+1)}$ in (3.16) at every iteration. The proof follows similar ideas as in [10]; the technical details are skipped for the sake of brevity.

Proposition 3.4. *Given cell-centered functions ϕ^n, ϕ^{n-1}, $\phi^{(m)}$, with $\|\phi^n\|_\infty$, $\left\|\phi^{n-1}\right\|_\infty < 1$, and $\overline{\phi^n} = \overline{\phi^{n-1}} = \overline{\phi^{(m)}} = \beta_0 < 1$, then there exists a unique solution $\phi^{(m+1)}$ to (3.16), with $\left\|\phi^{(m+1)}\right\|_\infty < 1$, and $\overline{\phi^{(m+1)}} = \beta_0$. Moreover, since ϕ^n, ϕ^{n-1} are discrete variables, there exists $0 < \delta_{n-1},\ \delta_n,\ \delta_{(m)} < \frac{1}{2}$, such that $\|\phi^n\|_\infty \le 1 - \delta_n$, $\left\|\phi^{n-1}\right\|_\infty \le 1 - \delta_{n-1}$ and $\left\|\phi^{(m)}\right\|_\infty \le 1 - \delta_{(m)}$. Then $\phi^{(m+1)}$ satisfies $\left\|\phi^{(m+1)}\right\|_\infty \le 1 - \delta_{(m+1)}$, where $\delta_{(m+1)} = \min(\frac{1}{2}, \hat{\delta})$ and $\hat{\delta}$ satisfies the following equality:*

$$\begin{aligned}
&\tau\left(\ln\frac{\hat{\delta}}{2-\hat{\delta}} - \ln\frac{1+\beta_0}{1-\beta_0}\right) + 4\epsilon^2 h^{-2}(1-\delta_{n-1}) + 4\theta_0 + 4\tau|\ln\delta_n| \\
&\quad + \ln(2-\delta_n) + 1 - \frac{G(\beta_0) - G(2-\delta_n)}{\beta_0 + \delta_n - 1} + \frac{G(\beta_0) - G(2-\delta_n)}{\delta_n - 1 - \beta_0} + C^* = 0,
\end{aligned} \tag{3.17}$$

where $C^* = \tau^{-1}C_1^{-2}h^{-\frac{d}{2}}(C_0 + \left\|\phi^{(m)} - \phi^n\right\|) + A$.

The main result of this section is stated below.

Theorem 3.1. *Given cell-centered functions ϕ^n, ϕ^{n-1}, with $\|\phi^n\|_\infty$, $\left\|\phi^{n-1}\right\|_\infty < 1$ and $\overline{\phi^n} = \overline{\phi^{n-1}} = \beta_0 < 1$, then there exists a unique cell-centered solution ϕ^{n+1} to (2.35)-(2.39), with $\left\|\phi^{n+1}\right\|_\infty < 1$, and $\overline{\phi^{n+1}} = \beta_0$.*

Proof. Clearly, given $\phi^{(0)} = \phi^n$, $\phi^{(1)}$ generated by (3.16) satisfies the equality (3.17). Since $\left\|\phi^{(1)}\right\|_\infty < 1$, we see that

$$C^* = \tau^{-1}C_1^{-2}h^{-\frac{d}{2}}(C_0 + \left\|\phi^{(0)} - \phi^n\right\|) + A \le \tau^{-1}C_1^{-2}h^{-\frac{d}{2}}(C_0 + 2\,|\Omega|^{\frac{1}{2}}) + A =: \hat{C}^*. \tag{3.18}$$

An induction application implies that $\left\|\phi^{(m)}\right\|_\infty < 1$, $\forall m \ge 0$. Then we can replace C^* by $\hat{C}^*$, and obtain a modified equality of (3.17), in which $\hat{\delta}$ is independent of m. Thus, if the sequence generated by (3.16) has a limit, say ϕ^{n+1}, then it must satisfy (3.17), with C^* replaced by $\hat{C}^*$. Then $\left\|\phi^{n+1}\right\|_\infty < 1 - \delta_{n+1}$, where $\delta_{n+1} = \min(\frac{1}{2}, \hat{\delta})$.

The rest work is focused on determining A to make $\mathcal{G}_h$ a contraction mapping, and the existence proof could be accomplished by taking $m \to +\infty$ on both sides of (3.16). Define the difference function between two consecutive iteration stages by:

$$\zeta^{(m)} := \phi^{(m)} - \phi^{(m-1)},\ \text{for } m \ge 1. \tag{3.19}$$

Since $\overline{\phi^{(m)}} = \overline{\phi^{(m-1)}} = \beta_0$, we infer that $\overline{\zeta^{(m)}} = 0$.

Taking a difference of (3.16) between the m^{th} and $(m+1)^{\text{st}}$, we get

$$\begin{aligned}
&\mathcal{G}_h(\phi^{(m+1)}) - \mathcal{G}_h(\phi^{(m)}) \\
&\quad = F_{1+\phi^n}(1+\phi^{(m+1)}) - F_{1+\phi^n}(1+\phi^{(m)}) - F_{1-\phi^n}(1-\phi^{(m+1)}) + F_{1-\phi^n}(1-\phi^{(m)}) \\
&\qquad + \tau\left(\ln(1+\phi^{(m+1)}) - \ln(1+\phi^{(m)}) - \ln(1-\phi^{(m+1)}) + \ln(1-\phi^{(m)})\right) \\
&\qquad + A\zeta^{(m+1)} - \frac{3}{4}\epsilon^2\Delta_h\zeta^{(m+1)} \\
&\quad = -\frac{1}{\tau}(\mathcal{L}_h^{CH})^{-1}(\zeta^{(m)}) + A\zeta^{(m)}.
\end{aligned} \tag{3.20}$$

Taking a discrete inner product with (3.20) by $\zeta^{(m+1)}$ yields

$$\begin{aligned}
&\left\langle F_{1+\phi^n}(1+\phi^{(m+1)}) - F_{1+\phi^n}(1+\phi^{(m)}) - F_{1-\phi^n}(1-\phi^{(m+1)}) + F_{1-\phi^n}(1-\phi^{(m)}), \zeta^{(m+1)} \right\rangle_c \\
&\quad + \tau \left\langle \ln(1+\phi^{(m+1)}) - \ln(1+\phi^{(m)}) - \ln(1-\phi^{(m+1)}) + \ln(1-\phi^{(m)}), \zeta^{(m+1)} \right\rangle_c \\
&\quad + A \left\langle \zeta^{(m+1)}, \zeta^{(m+1)} - \zeta^{(m)} \right\rangle_c + \frac{3}{4}\epsilon^2 \left\| \nabla_h \zeta^{(m+1)} \right\|_2^2 \\
&= -\frac{1}{\tau} \left\langle (\mathcal{L}_h^{CH})^{-1}(\zeta^{(m)}), \zeta^{(m+1)} \right\rangle_c .
\end{aligned} \tag{3.21}$$

By Lemma 2.2, as well as the monotonicity of $\ln(1+x) - \ln(1-x)$, the first two terms of (3.21) on the left side are always non-negative:

$$\begin{aligned}
&\left\langle F_{1+\phi^n}(1+\phi^{(m+1)}) - F_{1+\phi^n}(1+\phi^{(m)}) \right. \\
&\qquad \left. -F_{1-\phi^n}(1-\phi^{(m+1)}) + F_{1-\phi^n}(1-\phi^{(m)}), \zeta^{(m+1)} \right\rangle_c \geq 0,
\end{aligned} \tag{3.22}$$

$$\left\langle \ln(1+\phi^{(m+1)}) - \ln(1+\phi^{(m)}) - \ln(1-\phi^{(m+1)}) + \ln(1-\phi^{(m)}), \zeta^{(m+1)} \right\rangle_c \geq 0. \tag{3.23}$$

For the iteration relaxation term, an application of polarization identity leads to

$$\left\langle \zeta^{(m+1)}, \zeta^{(m+1)} - \zeta^{(m)} \right\rangle_c = \frac{1}{2} \left(\|\zeta^{(m+1)}\|^2 - \|\zeta^{(m)}\|_2^2 + \|\zeta^{(m+1)} - \zeta^{(m)}\|_2^2 \right). \tag{3.24}$$

The right hand side of (3.21), namely the term related to asymmetric operator $(\mathcal{L}_h^{CH})^{-1}$, could be analyzed as

$$\begin{aligned}
\left\langle (\mathcal{L}_h^{CH})^{-1}(\zeta^{(m)}), \zeta^{(m+1)} \right\rangle_c &= \left\langle (\mathcal{L}_h^{CH})^{-1}(\zeta^{(m)}), \zeta^{(m)} \right\rangle_c + \left\langle (\mathcal{L}_h^{CH})^{-1}(\zeta^{(m)}), \zeta^{(m+1)} - \zeta^{(m)} \right\rangle_c \\
&\geq \left\langle (\mathcal{L}_h^{CH})^{-1}(\zeta^{(m)}), \zeta^{(m+1)} - \zeta^{(m)} \right\rangle_c \\
&\geq -\left\| (\mathcal{L}_h^{CH})^{-1}(\zeta^{(m)}) \right\|_2 \cdot \|\zeta^{(m+1)} - \zeta^{(m)}\|_2 \\
&\geq -C_1^2 \|\zeta^{(m)}\|_2 \cdot \|\zeta^{(m+1)} - \zeta^{(m)}\|_2 \\
&\geq -\frac{\tau\epsilon^2}{4} C_1^2 \|\zeta^{(m)}\|_2^2 - \frac{C_1^{-6}}{\tau\epsilon^2} \|\zeta^{(m+1)} - \zeta^{(m)}\|_2^2 .
\end{aligned} \tag{3.25}$$

A combination of (3.22)-(3.25), along with the discrete elliptic regularity (3.10) to the higher order viscosity term, leads to

$$\begin{aligned}
&\left(\frac{A}{2} + \frac{3}{4} C_1^2 \epsilon^2 \right) \left\| \zeta^{(m+1)} \right\|_2^2 + \frac{A}{2} \left\| \zeta^{(m+1)} - \zeta^{(m)} \right\|_2^2 \\
&\qquad \leq \left(\frac{A}{2} + \frac{1}{4} C_1^2 \epsilon^2 \right) \left\| \zeta^{(m)} \right\|_2^2 + \frac{C_1^{-6}}{\tau^2 \epsilon^2} \left\| \zeta^{(m+1)} - \zeta^{(m)} \right\|_2^2 .
\end{aligned} \tag{3.26}$$

By taking $A \geq A_0 := 2C_1^{-6}\tau^{-2}\epsilon^{-2}$, a constant that may depend on τ, ϵ and Ω, we are able to obtain the following inequality:

$$\left(\frac{A}{2} + \frac{3}{4} C_1^2 \epsilon^2 \right) \left\| \zeta^{(m+1)} \right\|_2^2 \leq \left(\frac{A}{2} + \frac{1}{4} C_1^2 \epsilon^2 \right) \left\| \zeta^{(m)} \right\|_2^2 . \tag{3.27}$$

Thus the nonlinear iteration (3.16) is assured to be a contraction mapping, and the proof is complete. □

Remark 3.1. *At each nonlinear iteration, the asymmetric operator* $(\mathcal{L}_h^{CH})^{-1}(\phi^{m+1})$ *is replaced by a linear operator* $A\phi^{m+1}$*, so that the energy minimization technique can be used in the analysis. In fact, such a technique has been widely used in various gradient flows, including the Cahn-Hilliard equation with Flory-Huggins potential [6, 10, 18, 19, 50, 51], the liquid film droplet model [52], the Poisson-Nernst-Planck system [39, 40, 44], the reaction-diffusion system [38], etc. The convex nature of the singular energy part prevents the numerical solution approach the singular limit values of* ± 1*, which turns out to be the key point in the analysis.*

Remark 3.2. *Following similar ideas as in [6], we use a second order approximation nonlinear term in* (2.36) *to obtain energy stability, as will be demonstrated in the later section. Meanwhile, a nonlinear regularization term* $\tau\left(\ln(1+\phi^{(n+1)}) - \ln(1+\phi^n) - \ln(1-\phi^{(n+1)}) + \ln(1-\phi^n)\right)$ *is added in* (2.36) *to ensure the positivity preserving property (for the logarithmic arguments).*

Remark 3.3. *Though we derive a strict distance* δ_{n+1} *between the phase variable* ϕ^{n+1} *and* ± 1*,* δ_{n+1} *may depend on the following two distance* δ_n*,* δ_{n-1} *and so could converge to zero as* $n \to \infty$*. Therefore, a strict separation property of the numerical solution is not guaranteed in the positivity preserving analysis (for the logarithmic arguments). In other words, we do not obtain a uniform distance* δ *independent on* n*.*

Remark 3.4. *The existence of the numerical solution to* (2.35)-(2.39) *is unconditional, and there is no time step restriction for the existence. In more details, the existence and uniqueness for the iteration solution to* (3.16) *is unconditional, independent on the time step size* τ*, by Proposition 3.4. In turn, by taking* $m \to +\infty$*, the analysis presented in Theorem 3.1 reveals that, such an iteration is a contraction mapping, independent on the time step size* τ*. As a result, by passing the limit, the existence of the numerical solution to* (2.35)-(2.39) *is unconditional, without any time step restriction.*

4 Total energy stability analysis

Denote the discrete energy by

$$E_h(\phi) := \langle (1+\phi)\ln(1+\phi) + (1-\phi)\ln(1-\phi), \mathbf{1}\rangle_c - \frac{\theta_0}{2}\|\phi\|_2^2 + \frac{\epsilon^2}{2}\|\nabla_h\phi\|_2^2, \tag{4.1}$$

$$E_{h,total}(\phi, \mathbf{u}) := E_h(\phi) + \frac{1}{2\gamma}\|\mathbf{u}\|_2^2. \tag{4.2}$$

Then the main energy dissipation law is demonstrated in the following theorem.

Theorem 4.1. *For the proposed numerical scheme* (2.35)-(2.39)*, the following inequality holds for all* $n > 0$*:*

$$\tilde{E}_h(\phi^{n+1}, \phi^n, \boldsymbol{u}^{n+1}, p^{n+1}) + \frac{\tau\nu}{\gamma}\left\|\nabla_h \bar{\hat{\boldsymbol{u}}}^{n+\frac{1}{2}}\right\|_2^2 + \tau\left\|\nabla_h \mu^{n+\frac{1}{2}}\right\|_2^2 \le \tilde{E}_h(\phi^n, \phi^{n-1}, \boldsymbol{u}^n, p^n), \tag{4.3}$$

where

$$\begin{aligned}\tilde{E}_h(\phi^{n+1}, \phi^n, \boldsymbol{u}^{n+1}, p^{n+1}) = E_{h,total}(\phi^{n+1}, \boldsymbol{u}^{n+1}) + \frac{\tau^2}{8\gamma}\left\|p^{n+1}\right\|^2 + \frac{\theta_0}{4}\left\|\phi^{n+1}-\phi^n\right\|_2^2 \\ + \frac{\epsilon^2}{8}\left\|\nabla_h\left(\phi^{n+1}-\phi^n\right)\right\|_2^2.\end{aligned} \tag{4.4}$$

Proof. Taking a discrete inner product with (2.35) by $\bar{\hat{\mathbf{u}}}^{n+\frac{1}{2}} = \frac{1}{2}(\hat{\mathbf{u}}^{n+1} + \mathbf{u}^n)$ gives

$$\frac{\|\hat{\mathbf{u}}^{n+1}\|_2^2 - \|\mathbf{u}^n\|_2^2}{2\tau} + \left\langle \nabla_h p^n, \bar{\hat{\mathbf{u}}}^{n+\frac{1}{2}} \right\rangle_1 + \nu \left\| \nabla_h \bar{\hat{\mathbf{u}}}^{n+\frac{1}{2}} \right\|_2^2 + \gamma \left\langle \mathcal{A}_h \tilde{\phi}^{n+\frac{1}{2}} \nabla_h \mu^{n+\frac{1}{2}}, \bar{\hat{\mathbf{u}}}^{n+\frac{1}{2}} \right\rangle_1 = 0, \quad (4.5)$$

in which the summation-by-parts formula (2.30) has been applied:

$$\left\langle \bar{\tilde{\mathbf{u}}}^{n+\frac{1}{2}}, \tilde{\mathbf{u}}^{n+\frac{1}{2}} \cdot \nabla_h \bar{\hat{\mathbf{u}}}^{n+\frac{1}{2}} + \nabla_h \cdot \left(\bar{\tilde{\mathbf{u}}}^{n+\frac{1}{2}} (\tilde{\mathbf{u}}^{n+\frac{1}{2}})^T \right) \right\rangle_1 = 0. \quad (4.6)$$

Taking a discrete inner product with (2.38) by $\mathbf{u}^{n+1}$ leads to

$$\|\mathbf{u}^{n+1}\|_2 - \|\hat{\mathbf{u}}^{n+1}\|_2^2 + \|\mathbf{u}^{n+1} - \hat{\mathbf{u}}^{n+1}\|_2^2 = \|\mathbf{u}^{n+1}\|_2 - \|\bar{\hat{\mathbf{u}}}^{n+\frac{1}{2}}\|_2^2 + \frac{1}{4}\tau^2 \|\nabla_h (p^{n+1} - p^n)\|_2^2 = 0, \quad (4.7)$$

in which the summation by part formula (2.31) was used. In turn, a combination of (4.5) and (4.7) results in

$$\begin{aligned} \frac{\|\mathbf{u}^{n+1}\|_2^2 - \|\mathbf{u}^n\|_2^2}{2\tau} + \left\langle \nabla_h p^n, \bar{\hat{\mathbf{u}}}^{n+\frac{1}{2}} \right\rangle_1 + \frac{1}{8}\tau \|\nabla_h (p^{n+1} - p^n)\|_2^2 + \nu \left\| \nabla_h \bar{\hat{\mathbf{u}}}^{n+\frac{1}{2}} \right\|_2^2 \\ + \gamma \left\langle \mathcal{A}_h \tilde{\phi}^{n+\frac{1}{2}} \nabla_h \mu^{n+\frac{1}{2}}, \bar{\hat{\mathbf{u}}}^{n+\frac{1}{2}} \right\rangle = 0. \end{aligned} \quad (4.8)$$

For the pressure gradient term $\left\langle \nabla_h p^n, \bar{\hat{\mathbf{u}}}^{n+\frac{1}{2}} \right\rangle_1$, we make use of (2.38) and (2.39), so that $\nabla_h \cdot \hat{\mathbf{u}}^{n+1} = \frac{1}{2}\tau \Delta_h (p^{n+1} - p^n)$. This in turn results in

$$\begin{aligned} \left\langle \nabla_h p^n, \bar{\hat{\mathbf{u}}}^{n+\frac{1}{2}} \right\rangle_1 &= -\left\langle p^n, \nabla_h \cdot \bar{\hat{\mathbf{u}}}^{n+\frac{1}{2}} \right\rangle_c = -\frac{1}{2} \left\langle p^n, \nabla_h \cdot \hat{\mathbf{u}}^{n+1} \right\rangle_c \\ &= -\frac{1}{4}\tau \left\langle p^n, \Delta_h (p^{n+1} - p^n) \right\rangle_c = \frac{1}{4}\tau \left\langle \nabla_h p^n, \nabla_h (p^{n+1} - p^n) \right\rangle_1 \\ &= \frac{\tau}{8} (\|\nabla_h p^{n+1}\|_2^2 - \|\nabla_h p^n\|_2^2) - \frac{\tau}{8} \|\nabla_h (p^{n+1} - p^n)\|_2^2. \end{aligned} \quad (4.9)$$

As a consequence, a substitution of (4.9) into (4.8) yields

$$\begin{aligned} \frac{\|\mathbf{u}^{n+1}\|_2^2 - \|\mathbf{u}^n\|_2^2}{2\tau} + \frac{\tau}{8} (\|\nabla_h p^{n+1}\|_2^2 - \|\nabla_h p^n\|_2^2) + \nu \left\| \nabla_h \bar{\hat{\mathbf{u}}}^{n+\frac{1}{2}} \right\|_2^2 \\ + \gamma \left\langle \mathcal{A}_h \tilde{\phi}^{n+\frac{1}{2}} \nabla_h \mu^{n+\frac{1}{2}}, \bar{\hat{\mathbf{u}}}^{n+\frac{1}{2}} \right\rangle = 0. \end{aligned} \quad (4.10)$$

For the CH system, taking inner product with (2.36) by $\tau \mu^{n+\frac{1}{2}}$, and with (2.37) by $(\phi^{n+1} - \phi^n)$, we get

$$\begin{aligned} &\left\langle G(1+\phi^{n+1}) + G(1-\phi^{n+1}) - G(1+\phi^n) - G(1-\phi^n), 1 \right\rangle_c - \theta_0 \left\langle \tilde{\phi}^{n+\frac{1}{2}}, \phi^{n+1} - \phi^n \right\rangle_c \\ &+ \epsilon^2 \left\langle \nabla_h \bar{\bar{\phi}}^{n+\frac{1}{2}}, \nabla_h (\phi^{n+1} - \phi^n) \right\rangle_1 - \tau \left\langle \mathcal{A}_h \tilde{\phi}^{n+\frac{1}{2}} \nabla_h \mu^{n+\frac{1}{2}}, \bar{\hat{\mathbf{u}}}^{n+\frac{1}{2}} \right\rangle_1 + \tau \left\| \nabla_h \mu^{n+\frac{1}{2}} \right\|_2^2 \\ &+ \tau \left\langle \ln(1+\phi^{n+1}) - \ln(1+\phi^n) - \ln(1-\phi^{n+1}) + \ln(1-\phi^n), \phi^{n+1} - \phi^n \right\rangle_c = 0, \end{aligned} \quad (4.11)$$

with summation-by-parts formula (2.34) recalled. The linear expansive and surface diffusion terms

could be analyzed as follows:

$$
\begin{aligned}
&-\left\langle \tilde{\phi}^{n+\frac{1}{2}}, \phi^{n+1}-\phi^{n}\right\rangle_{c} = -\left\langle \frac{3}{2}\phi^{n+1}-\frac{1}{2}\phi^{n}, \phi^{n+1}-\phi^{n}\right\rangle_{c} \\
&\quad \geq -\frac{1}{2}(\|\phi^{n+1}\|_2^2-\|\phi^{n}\|_2^2)+\frac{1}{4}(\|\phi^{n+1}-\phi^{n}\|_2^2-\|\phi^{n}-\phi^{n-1}\|_2^2), \qquad (4.12)\\
&\left\langle \nabla_h \bar{\bar{\phi}}^{n+\frac{1}{2}}, \nabla_h(\phi^{n+1}-\phi^{n})\right\rangle_{1} = \left\langle \nabla_h(\frac{3}{4}\phi^{n+1}+\frac{1}{4}\phi^{n-1}), \nabla_h(\phi^{n+1}-\phi^{n})\right\rangle_{1} \\
&\quad = \frac{1}{2}\left\langle \nabla_h(\phi^{n+1}+\phi^{n}), \nabla_h(\phi^{n+1}-\phi^{n})\right\rangle_{1}+\frac{1}{4}\left\langle \nabla_h(\phi^{n+1}-2\phi^{n}+\phi^{n-1}), \nabla_h(\phi^{n+1}-\phi^{n})\right\rangle_{1} \\
&\quad \geq \frac{1}{2}\left(\|\nabla_h\phi^{n+1}\|_2^2-\|\nabla_h\phi^{n}\|_2^2\right)+\frac{1}{8}\left(\|\nabla_h(\phi^{n+1}-\phi^{n})\|_2^2-\|\nabla_h(\phi^{n}-\phi^{n-1})\|_2^2\right). \qquad (4.13)
\end{aligned}
$$

Using the monotonicity of $\ln(1+x)-\ln(1-x)$, we obtain

$$
\left\langle \ln(1+\phi^{n+1})-\ln(1+\phi^{n})-\ln(1-\phi^{n+1})+\ln(1-\phi^{n}), \phi^{n+1}-\phi^{n}\right\rangle_{c} \geq 0. \qquad (4.14)
$$

As a consequence, a substitution of (4.12)-(4.14) into (4.11) yields

$$
\begin{aligned}
&\left\langle G(1+\phi^{n+1})+G(1-\phi^{n+1})-G(1+\phi^{n})-G(1-\phi^{n}), 1\right\rangle_{c}-\frac{\theta_0}{2}(\|\phi^{n+1}\|_2^2-\|\phi^{n}\|_2^2) \\
&+\frac{\epsilon^2}{2}\left(\|\nabla_h\phi^{n+1}\|_2^2-\|\nabla_h\phi^{n}\|_2^2\right)+\frac{\theta_0}{4}(\|\phi^{n+1}-\phi^{n}\|_2^2-\|\phi^{n}-\phi^{n-1}\|_2^2)+\tau\left\|\nabla_h\mu^{n+\frac{1}{2}}\right\|_2^2 \qquad (4.15)\\
&+\frac{\epsilon^2}{8}\left(\|\nabla_h(\phi^{n+1}-\phi^{n})\|_2^2-\|\nabla_h(\phi^{n}-\phi^{n-1})\|_2^2\right)-\tau\left\langle \mathcal{A}_h\tilde{\phi}^{n+\frac{1}{2}}\nabla_h\mu^{n+\frac{1}{2}}, \bar{\hat{\mathbf{u}}}^{n+\frac{1}{2}}\right\rangle_{1}\leq 0,
\end{aligned}
$$

Finally, a combination of (4.10) and (4.15) results in the following energy estimate:

$$
\begin{aligned}
&E_{h,CH}^{n+1}-E_{h,CH}^{n}+\frac{\tau^2}{8\gamma}\left(\|\nabla_h p^{n+1}\|_2^2-\|\nabla_h p^{n}\|_2^2\right)+\frac{\theta_0}{4}\left(\left\|\phi^{n+1}-\phi^{n}\right\|_2^2-\left\|\phi^{n}-\phi^{n-1}\right\|_2^2\right) \\
&\quad+\frac{\epsilon^2}{8}\left(\left\|\nabla_h(\phi^{n+1}-\phi^{n})\right\|_2^2-\left\|\nabla_h(\phi^{n}-\phi^{n-1})\right\|_2^2\right) \qquad (4.16)\\
&\quad+\frac{\tau\nu}{\gamma}\left\|\nabla_h\bar{\hat{\mathbf{u}}}^{n+\frac{1}{2}}\right\|_2^2+\tau\left\|\nabla_h\mu^{n+\frac{1}{2}}\right\|_2^2\leq 0.
\end{aligned}
$$

This completes the proof of Theorem 4.1. □

With the above energy estimate, an induction application implies that

$$
E_h(\phi^{n}, \mathbf{u}^{n}) \leq \tilde{E}_h(\phi^{n}, \phi^{n-1}, \mathbf{u}^{n}, p^{n}) \leq \tilde{E}_h(\phi^{0}, \phi^{-1}, \mathbf{u}^{0}, p^{-1}) = E_h(\phi^{0}, \mathbf{u}^{0}), \qquad (4.17)
$$

by taking the initial extrapolation $\phi^{-1}=\phi^{0}$, $p^{-1}=p^{0}$. Then we obtain the following result.

Corollary 4.1. *For every positive integer n, the solutions ϕ^{n+1}, $\boldsymbol{u}^{n+1}$ of (2.36)-(2.39) satisfy the following estimate:*

$$
\left\|\nabla_h\phi^{n+1}\right\|_2\leq C, \quad \left\|\boldsymbol{u}^{n+1}\right\|_2\leq C, \qquad (4.18)
$$

where C only depends on the θ_0, ϵ, ν, $|\Omega|$ and the initial value ϕ^{0}, $\boldsymbol{u}^{0}$.

Remark 4.1. *The first order numerical scheme has been reported in [5], with the established theoretical properties. Meanwhile, a direct extension to the second order numerical accuracy, such as the BDF2 approach analyzed in [10] for the pure Cahn-Hilliard equation, would face a serious*

difficulty in the theoretical analysis. The modified BDF2 algorithm has its advantage to deal with the nonlinear logarithmic terms, associated with the singular and convex nature of these terms. In turn, the positivity-preserving analysis of the BDF2 method, for the pure phase field equation, follows essential the same ideas as in the first order scheme. However, for the BDF2 approach to the Cahn-Hilliard-Navier-Stokes system, the energy stability analysis would face a serious theoretical difficulty. Instead, we use a modified Crank-Nicolson approach, in which the second order approximation to the logarithmic terms does not preserve the singularity as the phase variables approach the singular limit values of ± 1*, while the nonlinear artificial regularization term preserves a singular nature. In turn, the positivity-preserving analysis is accomplished with the help of this nonlinear artificial regularization term, while the total energy stability analysis is derived on the Crank-Nicolson format, for the proposed second order scheme* (2.35)-(2.39).

Remark 4.2. *In the chemical potential expansion* (2.37) *of the proposed numerical scheme, a modified Crank-Nicolson approximation, namely* $\frac{3}{4}\phi^{n+1} + \frac{1}{4}\phi^{n-1}$*, is applied in the surface diffusion part. Such an alternate Crank-Nicolson approximation greatly enhances the numerical stability for nonlinear equations, in comparison with the standard Crank-Nicolson version,* $\frac{1}{2}(\phi^{n+1} + \phi^n)$*. This fact was first reported in [28] to deal with viscous Burgers' equation, and it has been extensively applied to various gradient flow [6, 9, 12, 15, 16, 30, 31] and fluid [11, 49] models, etc. This stability advantages have been verified by extensive numerical evidences, as well as the theoretical analyses. Such an improved numerical stability is expected to facilitate the convergence analysis of the proposed numerical scheme, as will be considered in future works.*

Remark 4.3. *The convergence analysis of the proposed numerical scheme* (2.35)-(2.39) *is expected to be highly challenging, due to the highly nonlinear and coupled nature of the numerical system. In addition, the singular feature of the phase variable as its value approaches to the singular limit values of* ± 1 *makes the analysis even more complicated. A theoretical justification of the convergence analysis and error estimate will be considered in our future works; some technical ideas in the related works [3, 4, 7, 15, 39, 41] could be similarly applied.*

5 Numerical test

In this section, we perform some numerical tests to demonstrate the robustness of the proposed numerical scheme. For the weak velocity-phase coupled numerical algorithm, a Picard iteration technique is used to accelerate the computational program. Meanwhile, the preconditioned steepest descent (PSD) method [25] is used to solve the Cahn-Hilliard system. Specifically, a linear operator

$$\mathcal{L}[\phi] := \frac{1}{\triangle t} - 2\Delta_h + \frac{3}{4}\epsilon^2 \Delta_h^2$$

is implemented to replace the original nonlinear equation. In turn, the operator is fixed at each iteration, and we can use the Fast Fourier Transform (FFT) to solve the system. For more details of the PSD iteration, see the related work of [5, 6, 8, 24, 52], etc.

5.1 Convergence test

To check the accuracy of the proposed scheme (2.35)-(2.39), we present two examples for both boundary conditions, either periodic or physical one. For simplicity, we take the kinematic viscosity as $\nu = 0.5$, surface diffusion parameter $\epsilon = 0.5$, and the expansive coefficient θ_0 is set as 3. For the

periodic case, the exact solutions are chosen to be

$$\phi(x,y,t) = 0.5\sin(2\pi x)\cos(2\pi y)\cos(t) + 0.1, \tag{5.1}$$

$$\mathbf{u} = \begin{pmatrix} -\cos(t)\cos(2\pi x)\sin(2\pi y) \\ \cos(t)\sin(2\pi x)\cos(2\pi y) \end{pmatrix}, \tag{5.2}$$

$$p = \sin(t)\sin(2\pi x). \tag{5.3}$$

Since the solution does not satisfy the original system (1.2)-(1.5), two artificial source terms have to be added to the right hand side of the Navier-Stokes equation (1.2) and the Cahn-Hilliard equation (1.3). We take $\tau = h$ to observe both the temporal and spatial accuracy orders, with $h = 2^{-k}$, $k = 4$, 5, 6 ,7, 8, 9. We choose the final time $T = 1$ and compare the exact and the computational solutions. Figure 1 (left) plots the numerical error of the phase variable, velocity and the pressure respect to the spatial size. A clear second order convergence is illustrated in this picture.

On the other hand, a slightly different result has been observed with physical boundary condition. In this case we choose the exact solutions as

$$\phi(x,y,t) = \frac{1}{\pi}\cos(\pi x)\cos(\pi y)\cos(t), \tag{5.4}$$

$$\mathbf{u} = \begin{pmatrix} -\cos(t)\sin(\pi x)^2\sin(2\pi y) \\ \cos(t)\sin(2\pi x)\sin(\pi y)^2 \end{pmatrix}, \tag{5.5}$$

$$p = \cos(t)\cos(2\pi x)\sin(2\pi y). \tag{5.6}$$

The parameters along with the spatial and temporal are all given as the same above. The associated convergence orders are reported in Figure 1 (right). It is clear that the velocity and phase variables remain to be second order convergent, while the accuracy order for the pressure variable is reduced to one. We remark that, by using pressure correction technique in (2.39) with boundary condition (2.41), an artificial Neumann boundary condition $\partial_n \left(p^{n+1} - p^n\right) = 0$ is implemented in (2.38), which induces a numerical boundary layer that prevents the scheme to be fully second order accurate; also see the related works of Shen [45, 46], Guermond, Minev and Shen [29], E and Liu [20–22], etc.

5.2 Buoyancy-driven flow

The Cahn-Hilliard-Navier-Stokes system can be used to simulate certain dynamics and observe the associated physical phenomena. We follow the idea in [13] and consider a single bubble rising in a box. An additional buoyancy force term $\mathbf{b}$ is added to the right hand side of the Navier-Stokes equation (1.2), shifting the original system as follows:

$$\mathbf{u}_t + (\mathbf{u}\cdot\nabla)\mathbf{u} - \nu\Delta\mathbf{u} - \nabla p + \phi\nabla\mu = \mathbf{b}, \tag{5.7}$$

$$\phi_t + \nabla\cdot(\phi\mathbf{u}) = \Delta\mu, \tag{5.8}$$

$$\mu = \ln(1+\phi) - \ln(1-\phi) - \theta_0\phi - \epsilon^2\Delta\phi, \tag{5.9}$$

$$\nabla\cdot\mathbf{u} = 0. \tag{5.10}$$

To be specific,

$$\mathbf{b} = (0, -b(\phi)^T), \quad b(\phi) = \lambda(\phi - \bar{\phi}),$$

and $\lambda = \frac{G(\rho_1-\rho_2)}{2}$, where G is the gravitational force and ρ_1 and ρ_2 denote the densities of the bubble and medium. We set the initial phase value as

$$\phi(x,y,0) = 0.9\tanh\left(\frac{\sqrt{(x-0.5)^2+(y-0.3)^2} - 0.25d}{\eta}\right), \tag{5.11}$$

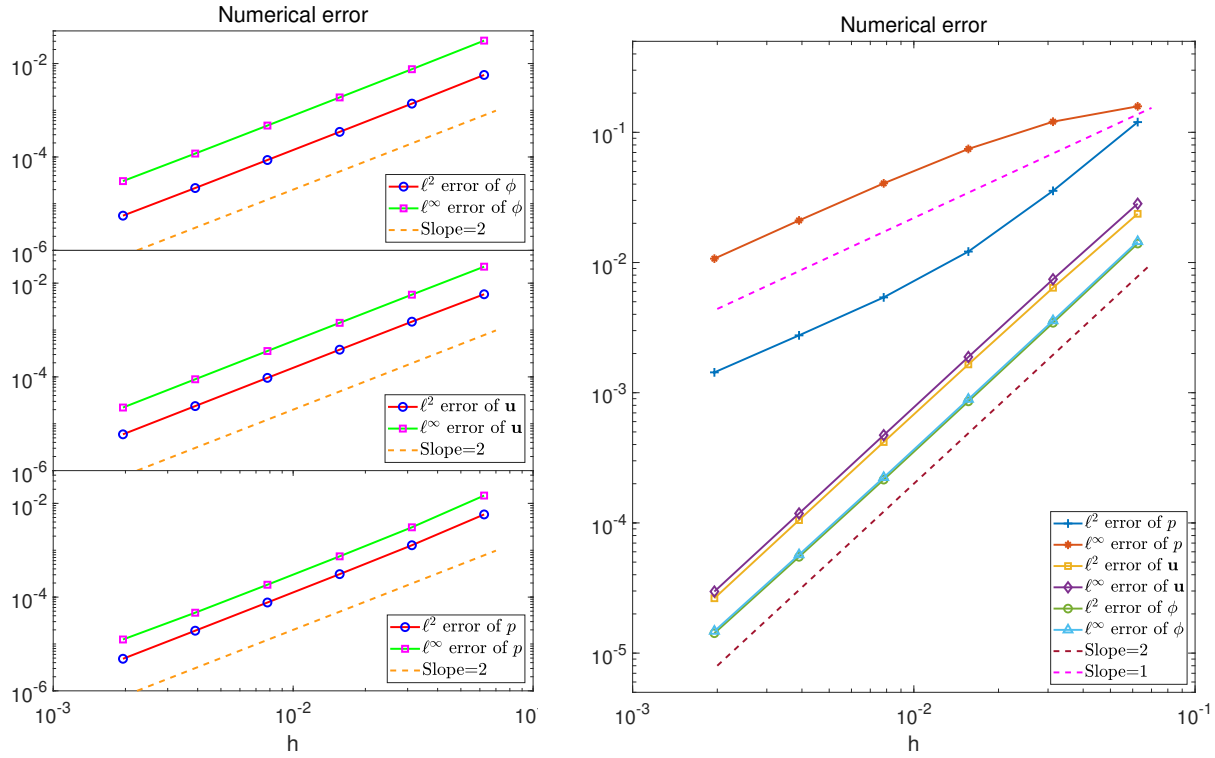

Figure 1: Numerical error of the phase variable, velocity field and pressure field. Periodic boundary case with initial value (5.1)-(5.3) is shown on the left, while the physical case with initial value (5.4)-(5.6) is demonstrated on the right. In the first case all three variables have the second order accuracy. In the physical boundary condition case, though the velocity and phase variables appear to be second order convergent, the pressure variable does not preserve a full second order accuracy.

where d controls the radius of the bubble and η represents the diffusive interfacial width. Here we choose $d = 0.5$ and $\eta = 0.01d$. The physical parameters are given by $\theta_0 = \frac{10\ln(19)}{9}$, so that the double wells of the potential are located at -0.9 and 0.9, and $\lambda = 20$, $\epsilon = 0.01$. The spatial and temporal sizes are set as $1/256$ and 0.0001, respectively. We consider the bubble rising under different viscosity parameters: $\nu = 0.1,\ 0.01,\ 0.001,\ 0.0001$. Figure 2 displays some snapshots in the above four cases. As ν becomes smaller, the convection term takes the lead and in turn the bubble rises faster, and deforms when reaching the boundary of the top side.

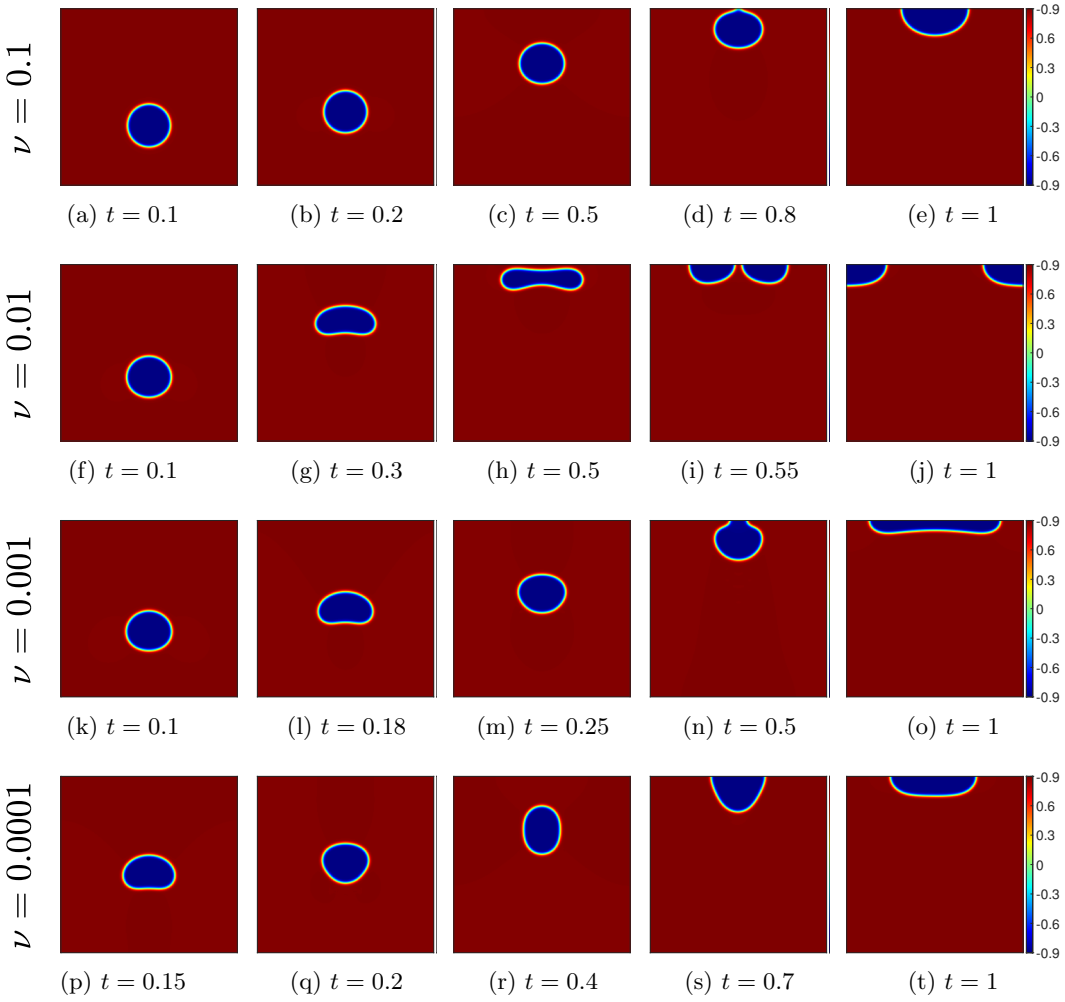

(a) $t = 0.1$ (b) $t = 0.2$ (c) $t = 0.5$ (d) $t = 0.8$ (e) $t = 1$

(f) $t = 0.1$ (g) $t = 0.3$ (h) $t = 0.5$ (i) $t = 0.55$ (j) $t = 1$

(k) $t = 0.1$ (l) $t = 0.18$ (m) $t = 0.25$ (n) $t = 0.5$ (o) $t = 1$

(p) $t = 0.15$ (q) $t = 0.2$ (r) $t = 0.4$ (s) $t = 0.7$ (t) $t = 1$

Figure 2: Bubble rises under different viscosity parameters, with different time snapshots.

5.3 Numerical simulation of the coarsening process

In this section we present the simulation results of the coarsening process, which illustrates that the proposed numerical scheme preserves the positivity property and total energy stability. A random initial value is chosen:

$$\phi_{i+\frac{1}{2},j+\frac{1}{2}} = 0.2 + 0.05\left(2r_{i+\frac{1}{2},j+\frac{1}{2}} - 1\right), \tag{5.12}$$

where $r_{i+\frac{1}{2},j+\frac{1}{2}}$ are uniform random numbers in $[0, 1]$. We further set the initial velocity as $\mathbf{u}^0 = 0$. The physical parameters are given by: $\nu = 0.01$, $\theta_0 = 3.6$ and a sequence of ϵ, $\epsilon = 0.01,\ 0.02,\ 0.03$.

The spatial size is still set as $h = 1/256$. Since the phase separation process will encounter a fast energy decay in the early time stage, we use a numerical strategy that slowly increases the time step sizes in the time evolution. Specifically, we set $\tau = 10^{-5}$ at the very beginning, and compute 1000 time steps, then use the time step size 2τ and repeat this process, until $\tau = 1.024 * 10^{-2}$. In other words, the time interval $[0, 0.01]$ will be simulated using the time step size $\tau = 10^{-5}$, then $T = [0.01, 0.03]$ with $\tau = 2 * 10^{-5}$, $T = [0.03, 0.07]$ with $\tau = 4 * 10^{-5}$, etc.

Figure 3 displays some pictures with different diffusion parameters, with its streamline plotted for the phase variable. As ϵ gets bigger, less topology structures are presented, and the separation process finishes faster. In Figure 4 we give the energy decay plot with different ϵ values, and an $O(t^{-\frac{1}{3}})$ dissipation rate is observed among these cases. It is noticed that, at the beginning time of each process, the original energy $E_{h,total}$ may not decrease, due to the random data singularity, while the modified energy $\tilde{E}_h$ always decreases over time, as proved in Theorem 4.1. Finally, Figure 6 presents the maximum and minimum values of ϕ in the time evolution. Of all three cases, the maximum value is lower than 0.9687, while the minimum value remains larger than -0.9598, which implies a strict separation property of the 2-D Cahn-Hilliard equation with logarithmic potential.

6 Conclusion

In this paper we have presented and analyzed a second order accurate numerical scheme for the Flory-Huggins-Cahn-Hilliard-Navier-Stokes system, with logarithmic energy potential. A modified Crank-Nicolson approximation is applied to the chemical potential, combined with a nonlinear artificial regularization term. For the convective term in the phase field evolutionary equation, the phase variable is evaluated by a second order extrapolation formula, while the velocity vector is updated by the Crank-Nicolson approximation. The Navier-Stokes equation is also computed by a similar semi-implicit method. The coupled numerical system creates a unique solution for the intermediate velocity field and the phase variable. The unique solvability and positivity-preserving analysis (for the logarithmic arguments) is accomplished by a nonlinear iteration process, in which the monotonicity analysis and the singularity analysis (as the phase variable approaches the singular limit values of -1 and 1) have played an essential role. After the intermediate velocity field is determined, a Helmholtz projection into the divergence-free vector field yields the velocity vector and the pressure variable at the next time step. As a result, the Stokes solver is decoupled, so that the numerical efficiency is greatly improved. For the full numerical system, a modified total energy stability of the proposed numerical scheme has been derived, with a few numerical correction terms included in the modified energy functional. Some numerical results are displayed, which demonstrate the robustness and efficiency of the proposed second order scheme.

Acknowledgments

This work is supported in part by the grants NSFC 12241101, 12071090 (W. Chen), NSF DMS-2012269 (C. Wang) and NSFC 12271237 (X. Wang). C. Wang also thanks the Key Laboratory of Mathematics for Nonlinear Sciences, Fudan University, for the support.

References

[1] F. Browder. Nonlinear elliptic boundary value problems. *Bull. Amer. Math. Soc.*, 69:962–874, 1963.

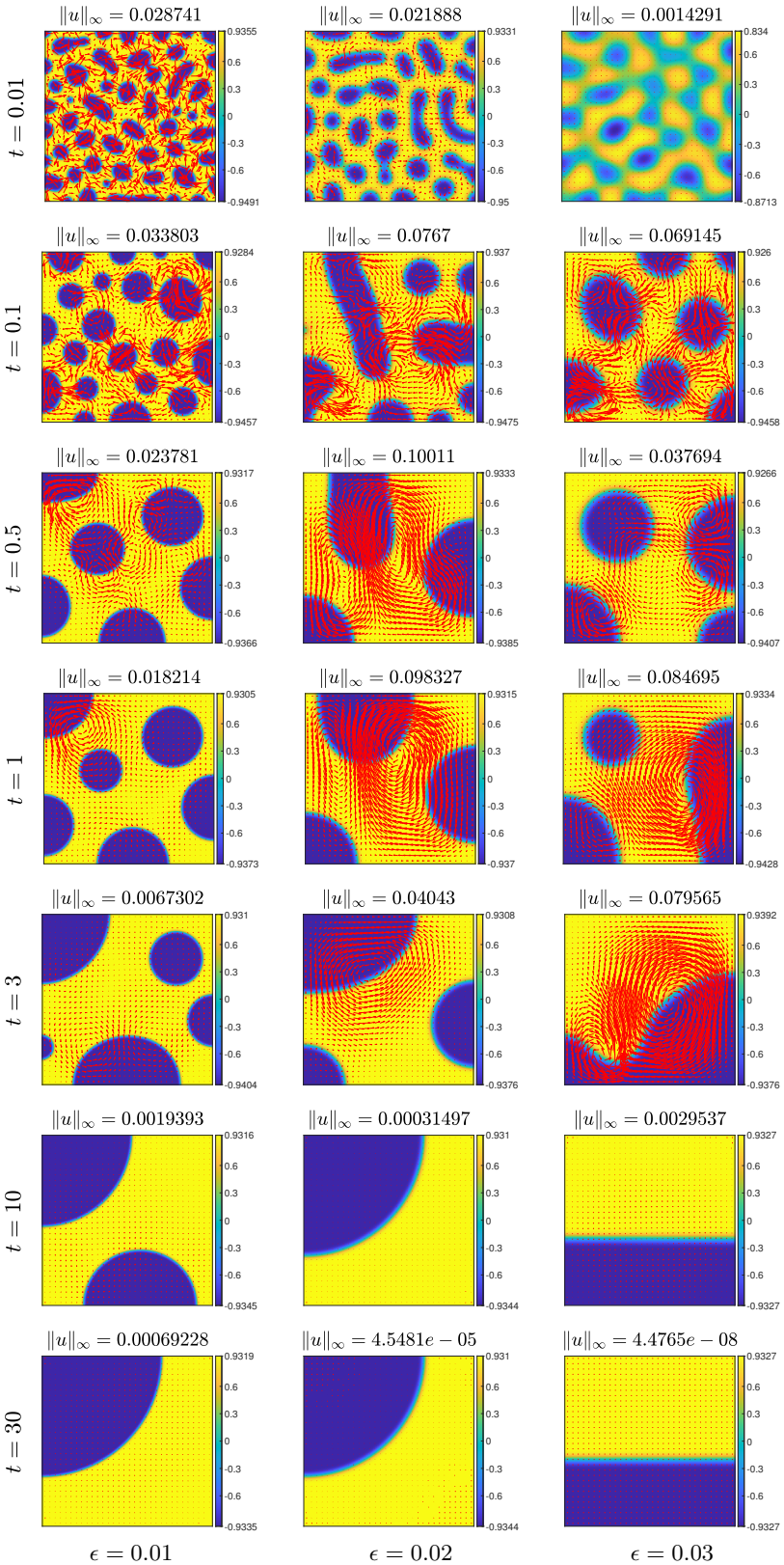

Figure 3: Numerical simulation of the coarsening process.

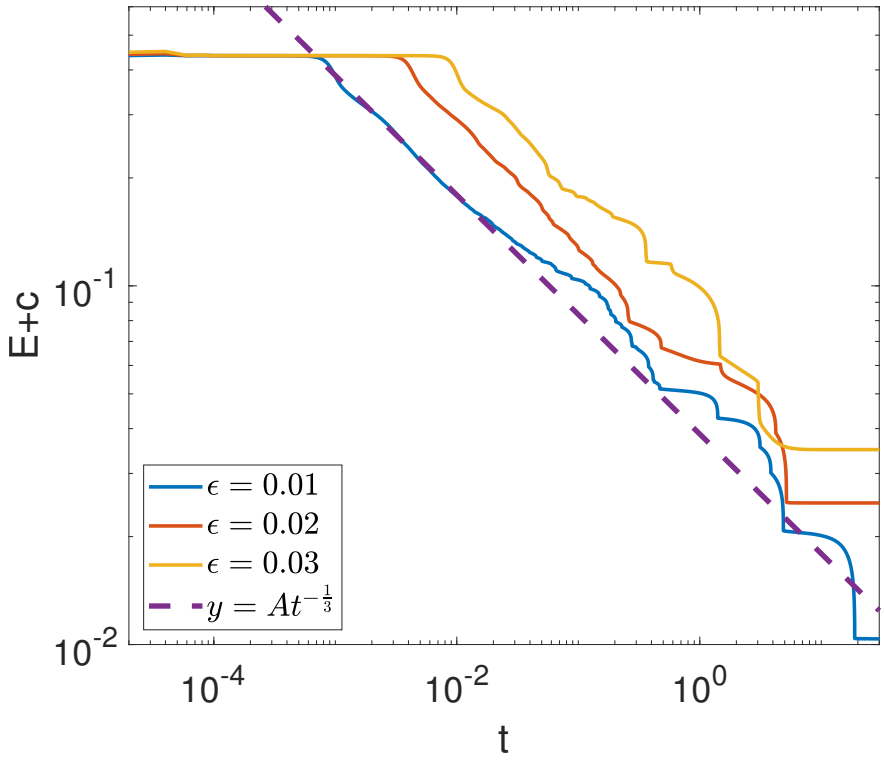

Figure 4: Energy decay under different diffusion parameters ϵ. All cases the energy strictly decreases. The $t^{-\frac{1}{3}}$ decay rate is also observed in the above simulation.

[2] J.W. Cahn, C.M. Elliott, and A. Novick-Cohen. The Cahn-Hilliard equation with a concentration dependent mobility: Motion by minus the Laplacian of the mean curvature. *Europ. J. Appl. Math.*, 7:287–301, 1996.

[3] W. Chen, W. Feng, Y. Liu, C. Wang, and S.M. Wise. A second order energy stable scheme for the Cahn-Hilliard-Hele-Shaw equation. *Discrete Contin. Dyn. Syst. Ser. B*, 24(1):149–182, 2019.

[4] W. Chen, D. Han, C. Wang, S. Wang, X. Wang, and Y. Zhang. Error estimate of a decoupled numerical scheme for the Cahn-Hilliard-Stokes-Darcy system. *IMA J. Numer. Anal.*, 42(3):2621–2655, 2022.

[5] W. Chen, J. Jing, C. Wang, and X. Wang. A positivity preserving, energy stable finite difference scheme for the Flory-Huggins-Cahn-Hilliard-Navier-Stokes system. *J. Sci. Comput.*, 92(2):31, 2022.

[6] W. Chen, J. Jing, C. Wang, X. Wang, and S.M. Wise. A modified Crank-Nicolson scheme for the Flory-Huggin Cahn-Hilliard model. *Commun. Comput. Phys.*, 31(1):60–93, 2022.

[7] W. Chen, Y. Liu, C. Wang, and S.M. Wise. An optimal-rate convergence analysis of a fully discrete finite difference scheme for Cahn-Hilliard-Hele-Shaw equation. *Math. Comp.*, 85:2231–2257, 2016.

[8] W. Chen, C. Wang, S. Wang, X. Wang, and S.M. Wise. Energy stable numerical schemes for ternary Cahn-Hilliard system. *J. Sci. Comput.*, 84:27, 2020.

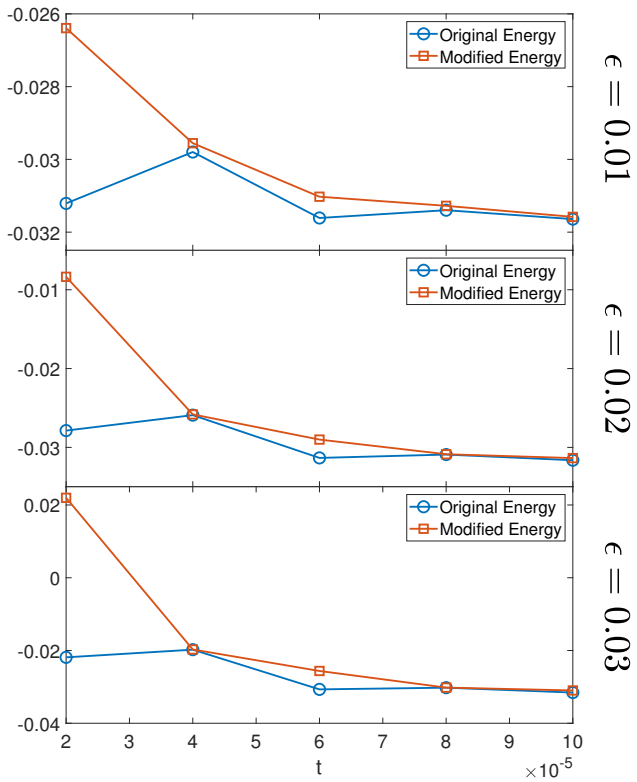

Figure 5: The original energy $E_{h,total}$, as defined in (4.2), versus the modified energy, as defined in (4.4) at the beginning of the time. The original energy may increase, while the modified energy remains decreasing.

[9] W. Chen, C. Wang, X. Wang, and S.M. Wise. A linear iteration algorithm for energy stable second order scheme for a thin film model without slope selection. *J. Sci. Comput.*, 59:574–601, 2014.

[10] W. Chen, C. Wang, X. Wang, and S.M. Wise. Positivity-preserving, energy stable numerical schemes for the Cahn-Hilliard equation with logarithmic potential. *J. Comput. Phys.: X*, 3:100031, 2019.

[11] K. Cheng and C. Wang. Long time stability of high order multi-step numerical schemes for two-dimensional incompressible Navier-Stokes equations. *SIAM J. Numer. Anal.*, 54:3123–3144, 2016.

[12] K. Cheng, C. Wang, S.M. Wise, and X. Yue. A second-order, weakly energy-stable pseudo-spectral scheme for the Cahn-Hilliard equation and its solution by the homogeneous linear iteration method. *J. Sci. Comput.*, 69:1083–1114, 2016.

[13] C. Collins, J. Shen, and S.M. Wise. An efficient, energy stable scheme for the Cahn-Hilliard-Brinkman system. *Commun. Comput. Phys.*, 13:929–957, 2013.

[14] M.I.M. Copetti and C.M. Elliott. Numerical analysis of the Cahn-Hilliard equation with a logarithmic free energy. *Numer. Math.*, 63:39–65, 1992.

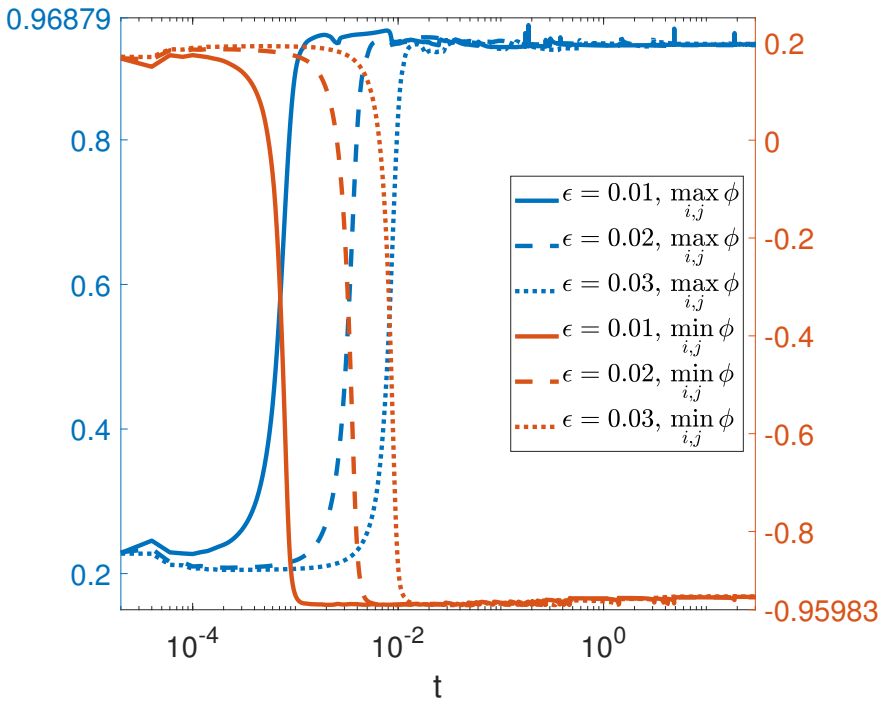

Figure 6: Maximum and minimum values of the phase variable along time under different ϵ.

[15] A. Diegel, C. Wang, X. Wang, and S.M. Wise. Convergence analysis and error estimates for a second order accurate finite element method for the Cahn-Hilliard-Navier-Stokes system. *Numer. Math.*, 137:495–534, 2017.

[16] A. Diegel, C. Wang, and S.M. Wise. Stability and convergence of a second order mixed finite element method for the Cahn-Hilliard equation. *IMA J. Numer. Anal.*, 36:1867–1897, 2016.

[17] M. Doi. *Soft Matter Physics.* Oxford University Press, Oxford, UK, 2013.

[18] L. Dong, C. Wang, H. Zhang, and Z. Zhang. A positivity-preserving, energy stable and convergent numerical scheme for the Cahn-Hilliard equation with a Flory-Huggins-deGennes energy. *Commun. Math. Sci.*, 17:921–939, 2019.

[19] L. Dong, C. Wang, H. Zhang, and Z. Zhang. A positivity-preserving second-order BDF scheme for the Cahn-Hilliard equation with variable interfacial parameters. *Commun. Comput. Phys.*, 28:967–998, 2020.

[20] W. E and J.-G. Liu. Projection method I: Convergence and numerical boundary layers. *SIAM J. Numer. Anal.*, 32:1017–1057, 1995.

[21] W. E and J.-G. Liu. Projection method II: Godunov-Ryabenki analysis. *SIAM J. Numer. Anal.*, 33:1597–1621, 1995.

[22] W. E and J.-G. Liu. Projection method III. Spatial discretization on the staggered grid. *Math. Comp.*, 71:27–47, 2002.

[23] C.M. Elliott and H. Garcke. On the Cahn-Hilliard equation with degenerate mobility. *SIAM J. Math. Anal.*, 27:404–423, 1996.

[24] W. Feng, Z. Guan, J.S. Lowengrub, C. Wang, S.M. Wise, and Y. Chen. A uniquely solvable, energy stable numerical scheme for the functionalized Cahn-Hilliard equation and its convergence analysis. *J. Sci. Comput.*, 76(3):1938–1967, 2018.

[25] W. Feng, A.J. Salgado, C. Wang, and S.M. Wise. Preconditioned steepest descent methods for some nonlinear elliptic equations involving p-Laplacian terms. *J. Comput. Phys.*, 334:45–67, 2017.

[26] X. Feng. Fully discrete finite element approximations of the Navier-Stokes-Cahn-Hilliard diffuse interface model for two-phase fluid flows. *SIAM J. Numer. Anal.*, 44:1049–1072, 2006.

[27] X. Feng and S.M. Wise. Analysis of a fully discrete finite element approximation of a Darcy-Cahn-Hilliard diffuse interface model for the Hele-Shaw flow. *SIAM J. Numer. Anal.*, 50:1320–1343, 2012.

[28] S. Gottlieb and C. Wang. Stability and convergence analysis of fully discrete Fourier collocation spectral method for 3-D viscous Burgers' equation. *J. Sci. Comput.*, 53:102–128, 2012.

[29] J. L. Guermond, P. Minev, and J. Shen. An overview of projection methods for incompressible flows. *Comput. Methods Appl. Mech. Engrg.*, 195:6011–6045, 2006.

[30] J. Guo, C. Wang, S.M. Wise, and X. Yue. An H^2 convergence of a second-order convex-splitting, finite difference scheme for the three-dimensional Cahn-Hilliard equation. *Commun. Math. Sci.*, 14:489–515, 2016.

[31] J. Guo, C. Wang, S.M. Wise, and X. Yue. An improved error analysis for a second-order numerical scheme for the Cahn-Hilliard equation. *J. Comput. Appl. Math.*, 388:113300, 2021.

[32] D. Han and X. Wang. A second order in time, uniquely solvable, unconditionally stable numerical scheme for Cahn-Hilliard-Navier-Stokes equation. *J. Comput. Phys.*, 290:139–156, 2015.

[33] F. Harlow and J. Welch. Numerical calculation of time-dependent viscous incompressible flow of fluid with free surface. *Phys. Fluids*, 8:2182–2189, 1965.

[34] D. Kay and R. Welford. Efficient numerical solution of Cahn-Hilliard-Navier-Stokes fluids in 2D. *SIAM J. Sci. Comput.*, 29:2241–2257, 2007.

[35] J.S. Kim, K. Kang, and J.S. Lowengrub. Conservative multigrid methods for Cahn-Hilliard fluids. *J. Comput. Phys.*, 193:511–543, 2003.

[36] C. Liu and J. Shen. A phase field model for the mixture of two incompressible fluids and its approximation by a Fourier-spectral method. *Physica D*, 179:211–228, 2003.

[37] C. Liu, J. Shen, and X. Yang. Decoupled energy stable schemes for a phase-field model of two-phase incompressible flows with variable density. *J. Sci. Comput.*, 62(2):601–622, 2015.

[38] C. Liu, C. Wang, and Y. Wang. A structure-preserving, operator splitting scheme for reaction-diffusion equations with detailed balance. *J. Comput. Phys.*, 436:110253, 2021.

[39] C. Liu, C. Wang, S.M. Wise, X. Yue, and S. Zhou. A positivity-preserving, energy stable and convergent numerical scheme for the Poisson-Nernst-Planck system. *Math. Comp.*, 90:2071–2106, 2021.

[40] C. Liu, C. Wang, S.M. Wise, X. Yue, and S. Zhou. An iteration solver for the Poisson-Nernst-Planck system and its convergence analysis. *J. Comput. Appl. Math.*, 406:114017, 2022.

[41] Y. Liu, W. Chen, C. Wang, and S.M. Wise. Error analysis of a mixed finite element method for a Cahn-Hilliard-Hele-Shaw system. *Numer. Math.*, 135:679–709, 2017.

[42] J.S. Lowengrub and L. Truskinovsky. Cahn-Hilliard fluids and topological transitions. *Proc. R. Soc. Lond. A*, 454:2617–2654, 1998.

[43] G. Minty. On a monotonicity method for the solution of non-linear equations in Banach spaces. *Proc. Nat. Acad. Sci.*, 50:1038–1041, 1963.

[44] Z. Qiao and S. Sun. Two-phase fluid simulation using a diffuse interface model with Peng-Robinson equation of state. *SIAM J. Sci. Comput.*, 36(4):B708–B728, 2014.

[45] J. Shen. On error estimates of projection methods for Navier-Stokes equations. first-order schemes. *SIAM J. Numer. Anal.*, 29(1):57–77, 1992.

[46] J. Shen. On error estimates of the projection methods for the Navier-Stokes equations: Second-order schemes. *Math. Comp.*, 65(215):1039–1065, 1996.

[47] J. Shen and X. Yang. A phase-field model and its numerical approximation for two-phase incompressible flows with different densities and viscosities. *SIAM J. Sci. Comput.*, 32:1159–1179, 2010.

[48] J. Shen and X. Yang. Decoupled, energy stable schemes for phase-field models of two-phase incompressible flows. *SIAM J. Numer. Anal.*, 53(1):279–296, 2015.

[49] C. Wang, J. Wang, Z. Xia, and L. Xu. Optimal error estimates of a second-order projection finite element method for magnetohydrodynamic equations. *Math. Model. Numer. Anal.*, 56(3):767–789, 2022.

[50] M. Yuan, W. Chen, C. Wang, S.M. Wise, and Z. Zhang. An energy stable finite element scheme for the three-component Cahn-Hilliard-type model for macromolecular microsphere composite hydrogels. *J. Sci. Comput.*, 87:78, 2021.

[51] M. Yuan, W. Chen, C. Wang, S.M. Wise, and Z. Zhang. A second order accurate in time, energy stable finite element scheme for the Flory-Huggins-Cahn-Hilliard equation. *Adv. Appl. Math. Mech.*, 14(6):1477–1508, 2022.

[52] J. Zhang, C. Wang, S.M. Wise, and Z. Zhang. Structure-preserving, energy stable numerical schemes for a liquid thin film coarsening model. *SIAM J. Sci. Comput.*, 43(2):A1248–A1272, 2021.

[53] J. Zhao. A general framework to derive linear, decoupled and energy-stable schemes for reversible-irreversible thermodynamically consistent models. *Comput. Math. Appl.*, 110(5):91–109, 2022.

[54] J. Zhao and D. Han. Second-order decoupled energy-stable schemes for Cahn-Hilliard-Navier-Stokes equations. *J. Comput. Phys.*, 443:110536, 2021.

[55] J. Zhao, X. Yang, J. Shen, and Q. Wang. A decoupled energy stable scheme for a hydrodynamic phase-field model of mixtures of nematic liquid crystals and viscous fluids. *J. Comput. Phys.*, 305:539–556, 2016.